Contents

1 Introduction

The development of human society has always been closely connected to searching new energy sources. In present time, the main ways of gaining energy is burning the fossil fuels like coal and petroleum, nuclear fission of heavy atoms like uranium-235 and also the exploitation of renewable sources like wind, water or sun. However, none of these energy sources is perfect. The fossil fuels cause massive pollution of Earth's atmosphere by CO_2 and therefore contribute to the greenhouse effect and also their reserves are limited. The exploitation of the renewable sources is limited by local geographic and weather conditions. Presently the most promising nuclear fission faces problems with storing of the radioactive waste. These disadvantages along with quick population growth (world population is expected to reach almost 8.1 billion in 2030) and also growth of the global primary energy demand (projected to increase by 52% from 2003 to 2030) are the main arguments adverting to the necessity of finding a new, efficient energy source available for all nations and harmless to the environment.

1.1 Nuclear fusion

The nuclear fusion is a reaction between two atomic nuclei of light atoms (like hydrogen or helium), which unite to create a heavier atomic nuclei. The new nuclear arrangement is more stable, its total mass is reduced, and therefore corresponding amount of energy is released. This energy is in form of kinetic energy of the products. The amount of released energy is far greater than by nuclear fission of heavy atoms as you can see on Fig.1.1. [1] [5] [16]

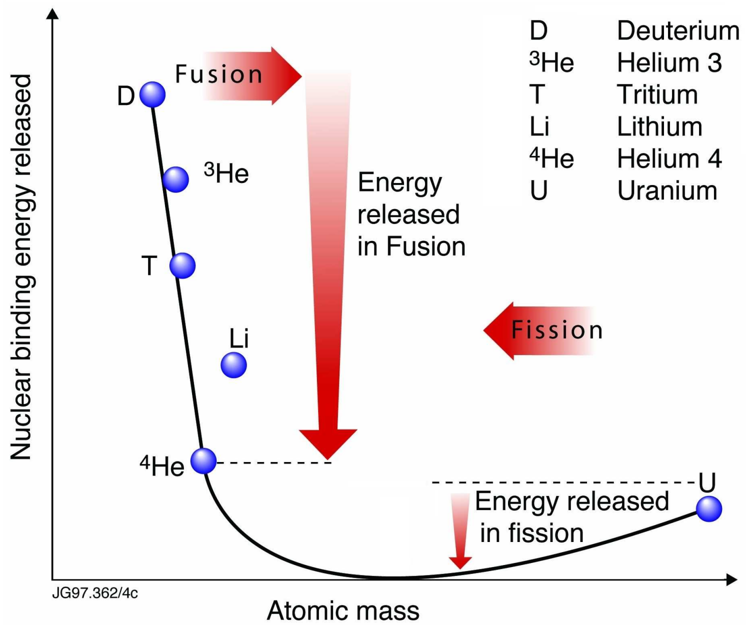

Figure 1.1: Energy released by nuclear reactions [16]

There are several reactions, which may be used for controlled nuclear fusion on Earth [2]:

$$D + T \rightarrow {}^{4}He\ (3.52\ MeV) + n\ (14.06\ MeV) \tag{1.1}$$

$$D + D \rightarrow T\ (1.01\ MeV) + p\ (3.03\ MeV) \tag{1.2}$$

$$D + D \rightarrow {}^{3}He\ (0.82\ MeV) + n\ (2.45\ MeV) \tag{1.3}$$

$$D + {}^{3}He \rightarrow {}^{4}He\ (3.67\ MeV) + p\ (14.67\ MeV) \tag{1.4}$$

The first of these reactions (1.1) is supposed to be used in the first generation thermonuclear reactors, as it is the easiest to achieve. It is a reaction between two isotopes of hydrogen, deuterium and tritium (DT reaction). For lower energies the probability (cross section) of DT fusion reaction is much higher than the probabilities of other mentioned reactions. [1]

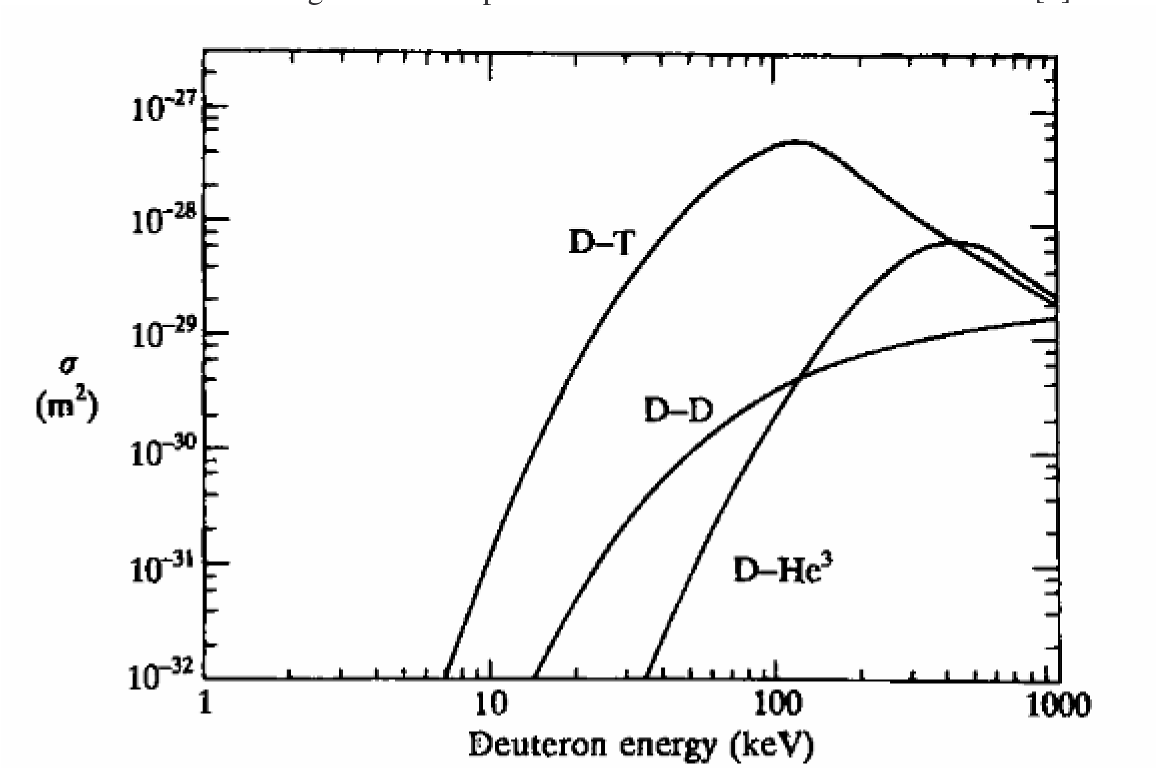

Figure 1.2: Nuclear reactions cross sections, the two D-D reactions have similar cross sections, the graph shows their sum [5]

Tritium is radioactive with a half-life of 12.3 years and so its natural reserves are negligible. Therefore it has to be manufactured. It is projected that tritium will be produced in the future fusion power plants by reaction of lithium with neutrons released by the fusion reaction:

$${}^{6}Li + n \rightarrow {}^{4}He + T + 4.8\ MeV \tag{1.5}$$

$${}^{7}Li + n \rightarrow {}^{4}He + T + n - 2.5\ MeV \tag{1.6}$$

Deuterium can be gained easily from the sea water. The Earth's reserves of lithium are estimated in millions of tons and will last for at least thousand years. The reserves of deuterium are practically inexhaustible.

As we can see, the nuclear fusion could be an ideal future energy source. The fuel is abundant and its reserves are widely distributed on Earth. The reaction by-product, helium, is a harmless inert gas, therefore there will be no radioactive waste and no pollution of the atmosphere.

1.2 Plasma

For fusion reaction to occur, it is necessary to bring the two nuclei very close together. It is therefore necessary to overcome their strong electrostatic repulsive force. The method which seems to be the most effective to increase the probability for the two nuclei of getting close enough to react is to warm their gas mixture. To ensure fusion in sufficient rate, temperatures of hundreds of millions Kelvins are needed. In these extreme temperatures, the gas is fully ionized and we refer to it as plasma or “the fourth state of matter“.

“Plasma is a quasi-neutral gas of charged and neutral particles, which shows a collective behaviour“ [2].

Plasmas are quasi-neutral, which means that local charge concentrations or external potentials are shielded out on distances short enough in comparison with the plasma dimensions. Parameter which describes the rate of shielding in plasma is called the Debye length λ_D:

$$\lambda_D = \left(\frac{\varepsilon_0 k T_e}{n_e e^2} \right)^{1/2} \qquad \text{[SI]} \tag{1.7}$$

where $\varepsilon_0 = 8.85 \cdot 10^{-12} kg^{-1} m^{-3} s^4 A^2$ is the permittivity of vacuum, $k = 1.38 \cdot 10^{-23} m^2 kg \cdot s^{-2} K^{-1}$ is the Boltzmann constant, T_e is the electron temperature, n_e is the electron density and $e = 1.6 \cdot 10^{-19} A \cdot s$ is the charge of electron. Therefore the total positive charge contained in plasma is approximately equal to the absolut value of the total negative charge.

Collective behaviour of the plasma particles means that the particles movement and trajectories are influenced not only by local conditions, but also by conditions in other places of the plasma. Plasma is a gas ionized in such extent, that its properties and particle movement is determined mainly by the electromagnetic forces and only marginally by collisions with neutral atoms. More information about plasma and its properties can be found in [5] [13] and especially in [2].

1.3 Ignition

One of the most important questions is what conditions need to be ensured to gain positive power balance from the thermonuclear fusion. The released fusion power must be greater than power needed to heat and confine the plasma. The first man to formulate these conditions mathematically was British physicist John Lawson. His famous Lawson criterion pointed out that product of plasma density and energy confinement time must exceed certain value. Plasma density n is a number of ions per cubic metre and the energy confinement time τ_E describes the rate of plasma energy losses and is defined as a ratio of total energy contained in plasma and total power of losses.

For a DT fusion, the reaction products are helium nuclei (called alpha particles) and neutrons. In case of magnetic confinement of the plasma, the alpha particles, being charged, are trapped within the magnetic field. They pass their energy in collisions to the plasma particles thus heating the plasma. With the rise of temperature the rate of fusion reactions increases and therefore also alpha particles heating is greater. Ignition is a desired state, when the alpha particles deliver all the heating power needed and the reaction is self-sustaining. The criterion for ignition in magnetically confined plasmas is similar to the Lawson criterion:

$$n \cdot \tau_E > \frac{12}{\langle \sigma v \rangle} \cdot \frac{T}{\mathrm{E}_\alpha} \quad [m^{-3}.s] \tag{1.8}$$

where n is the plasma ion density, τ_E energy confinement time, $<\sigma v>$ describes the fusion reaction rate, T is the plasma temperature and E_α energy of one alpha particle (3.5 *MeV*). The right side of the equation (1.8) is function of temperature only and this dependence has its minimum near 30 *keV*.

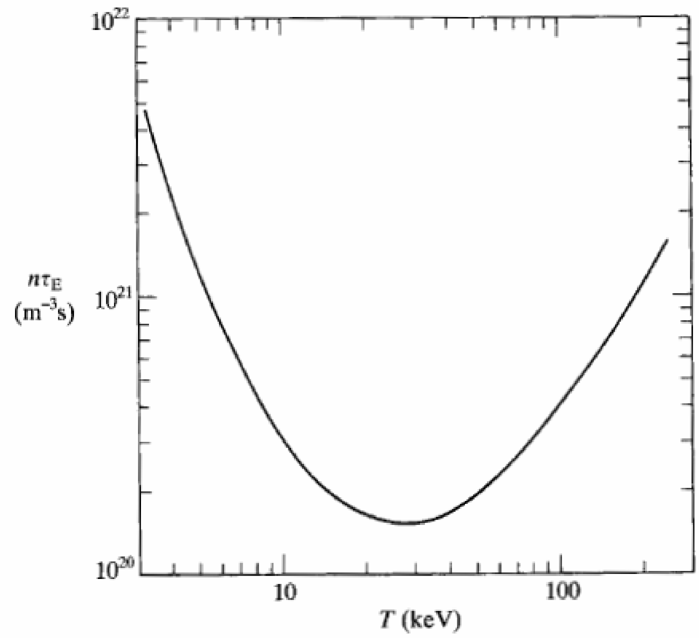

Figure 1.3: The condition for ignition - dependence of the needed product of density and energy confinement time on temperature [18]

However, because plasma averaged cross section <σv> and also the energy confinement time are functions of temperature, the ideal temperature to achieve ignition is lower. In the temperature range of 10-20 *keV*, the ignition criterion can be written as:

$$n \cdot T \cdot \tau \ > 3 \cdot 10^{21} m^{-3} \cdot keV \cdot s \tag{1.9}$$

The left side of equation (1.9) is sometimes reffered as *fusion triple product*. [1] [5] [6]

1.4 Plasma confinement

There are generally two principles of confining hot plasmas with ambition of achieving the required conditions mentioned above. These are magnetic and inertial confinement.

Magnetic confinement: Hot plasma contains charged particles, therefore can be confined by a strong magnetic field. Charged particles circle around the magnetic field lines with a specific radius called Larmor radius:

$$r_L = \frac{m \cdot v_\perp}{|q| \cdot B} \tag{1.10}$$

where m is the particle mass, $v_\perp$ is the particle velocity perpendicular to the magnetic field, q is the charge of the particle and B is the magnetic induction.
Plasma is kept in a closed volume and its typical parameters are τ_E ~ 1s and n ~ 10^{20} m^{-3} (lower densities and very high energy confinement times).

Inertial confinement: Very energetic laser pulses symmetrically heat a target sphere of DT. The target implodes and in its center the conditions for a fusion reaction are obtained. This approach features high densities of n ~ 10^{32} m^{-3} and very short energy confinement of typically τ_E ~ 10^{-11}s.

In linear magnetic field devices the end losses of particles and energy are too high, so it is necessary to enclose the magnetic field lines. Toroidally shaped devices satisfy this condition. However, in a system with toroidal magnetic field only, the magnetic field curvature and gradient result in an opposite vertical drift movement of ions and electrons and occurance of electric current. Resulting electric field causes ExB drift in outward direction:

$$\vec{v}_E = \frac{\vec{E} \times \vec{B}}{B^2} \tag{1.11}$$

To avoid the particles quickly drift away, it is necessary to twist the magnetic field lines, so that the resulting magnetic field is helical. There are two main types of magnetic devices solving this problem: stellarators and tokamaks.
Stellarator uses external coils wound around the plasma torus to twist the magnetic field. Tokamak uses induced plasma current in toroidal direction to create poloidal magnetic field and therefore to twist the magnetic field.

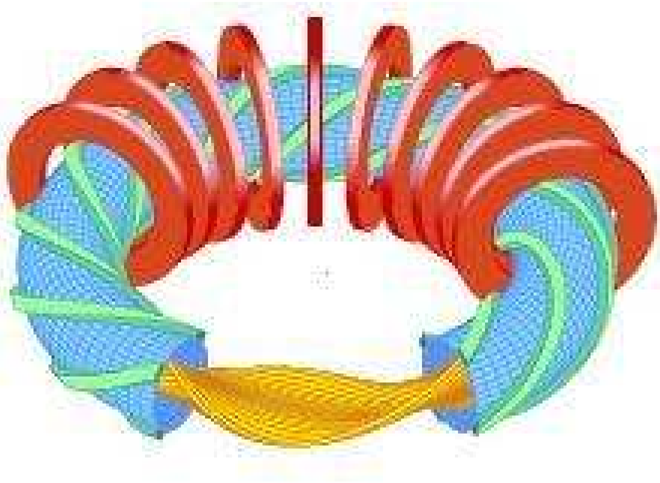

Figure 1.4: Scheme of a classical stellarator. It consists of the toroidal field coils (red), independent helical coils (green) and the vacuum vessel (blue). [6]

1.5 Tokamak

Tokamak (toroidalnaja kamera s magnitnymi katuškami) is the most advanced device confining hot plasma in the fusion research. It was projected in the fifth decade of 20th century in Moscow, USSR. It is generally a toroidal shaped vacuum vessel with strong toroidal field and weaker poloidal field. Toroidal field is produced by coils surrounding the vacuum vessel. Plasma in tokamak acts as secondary single-turn winding of a transformer. Strong induced current heats the plasma and creates the poloidal magnetic field, thus twisting the toroidal field lines. Resultant helically shaped magnetic field lines cause that each particle spends similar time both in the high and low toroidal field regions. Therefore the drifts responsible for charge separation last only for a short time before being reversed and in time average their effect is cancelled. Additional outer poloidal field coils help to shape and position plasma.

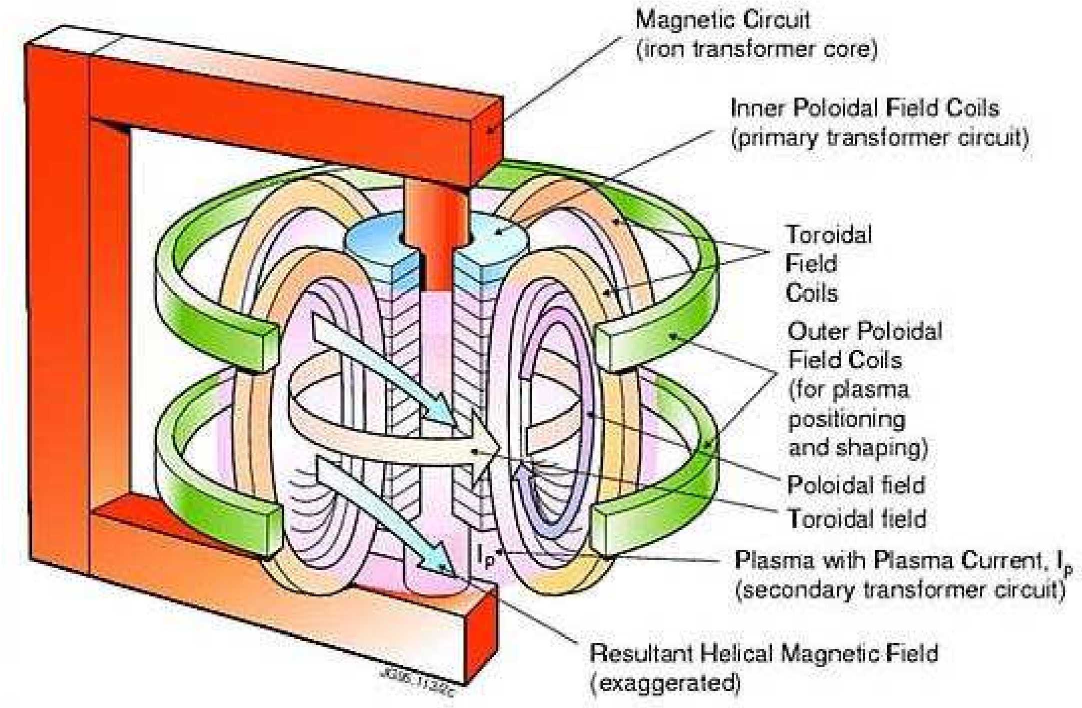

Figure 1.5: Scheme of a tokamak [17]

The vacuum vessel has two symmetry axes, major and minor. These axes characterize two basic directions: toroidal and poloidal. Basic tokamak geometrical parameters are major radius *R* and minor radius *a*. Major radius is a distance between major and minor axis and minor radius is a shortest distance between minor axis and edge of the vessel (see Fig.1.6). The helicity of magnetic field in a tokamak is described by a parameter called *safety factor q*. It is a number of toroidal turns of the magnetic field line needed to encircle one poloidal turn.

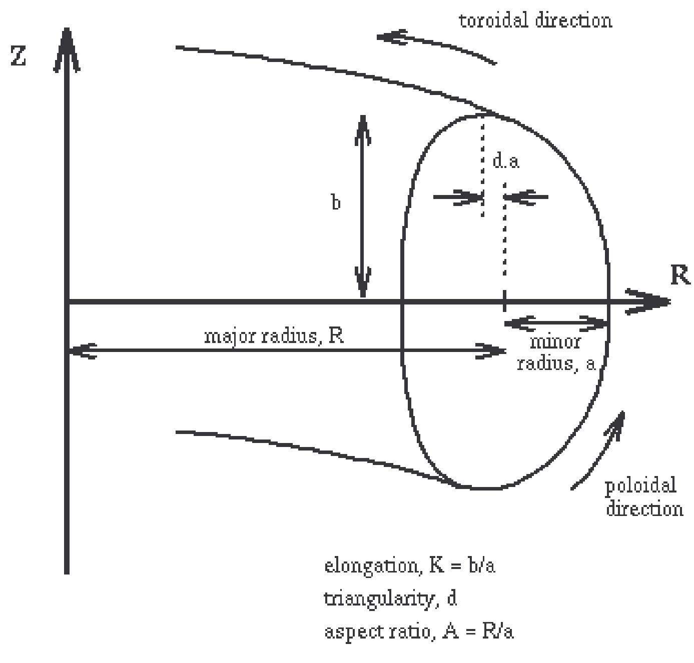

Figure 1.6: Tokamak geometry [19]

In a tokamak, continuous heat source must exist to initially heat the plasma to the needed temperatures and then to maintain these temperatures and balance the energy losses of plasma. There are several ways of heating the plasma in tokamak. Initial ohmic heating is caused by induced toroidal current I_p. However, as the plasma temperature rises, efficiency of this method of heating quickly decreases. This is caused by increasing plasma conductivity. Therefore additional heating methods must be used.

Neutral beam injection (NBI): Injection of energetic neutral particles into the plasma column. Ions are accelerated and then neutralized, so they are not affected by the tokamak magnetic field and are able to access deeper parts of the plasma. There the neutral atoms are ionized, caught by the magnetic field and they pass their energy to the plasma particles via collisions.

Ion cyclotron resonance heating (ICRH): Emitted electromagnetic waves of certain frequency (tens of MHz) resonate with the cyclotron motion of the plasma ions. This method of heating has the advantage of being localised at a particular location.

Self-heating of plasma: As I already mentioned, alpha particles produced by the fusion reaction help to heat the plasma by collisions with plasma particles. The moment when all heating needed is delivered only by the alpha particles is called *ignition*.

Current research of the tokamak plasmas faces many problems. Plasmas are the source of numerous instabilities which lead to a deterioration of the energy and particle confinement. Also suitable materials of the components of a tokamak must be developed, to withstand extreme neutron fluxes and magnetic fields and not to be source of impurities released into the plasma.

1.6 JET, ITER and future

JET (Joint European Torus) is the largest operating nuclear fusion facility in the world. It is located in Culham, United Kingdom. JET tokamak started to operatate in 1983 and was the first fusion device to achieve a significant production of a fusion power. It holds several experimental records in fusion research, including 16 *MW* of peak fusion power.
The typical parameters of the JET tokamak are shown in the table below:

Plasma major radius	*2.96 m*
Plasma minor radius	*2.10 m* (vertical) *1.00 m* (horizontal)
Toroidal magnetic field (on plasma axis)	$\leq 3.45\ T$
Plasma current	$\leq 4.8\ MA$
Additional heating power	$\leq 25\ MW$

Table 1.1: Main JET tokamak parameters

Experimental results on tokamaks showed, that conditions needed for ignition can be achieved by increasing of the plasma minor radius and magnetic field (and consequently the plasma current). It was sufficiently demonstrated, that fusion as a power source is possible. Now it is necessary to build larger device technically on the same level as future power plant to prove the technical feasibility of fusion. The international fusion community has designed a *next* *step* device, called ITER, to fulfill this task. In June 2005, it was decided to construct ITER in Cadarache, France and on 21st November 2006 a Joint Implementation agreement was signed, thus establishing the ITER organization. It is projected to reach the *power amplification factor* of 10 (ratio of fusion power to the heating power) and gain necessary experimental data to design and operate the first fusion power plant. The first plasma experiments should be possible on ITER by the end of year 2016. The possible success of ITER would lead to construction of DEMO, a fully functional prototype of a fusion power plant producing electricity and then to first commercial devices.

2 Fuelling of tokamak plasmas

For present day and future devices, pellet injection has become a leading technique for plasma fuelling and also for controlling the plasma. Therefore I will aim my work at this method. Now I will only very briefly mention other possible ways of refuelling the plasma:

Gas puff: Gas puff is a method commonly used at tokamaks. It is a way of edge plasma fuelling. The neutral gas of deuterium and/or tritium is simply pumped into the vacuum vessel. However, in larger devices and hotter and denser plasmas, only a small fraction of neutral gas particles will be able to penetrate across the separatrix and it will not be possible to use gas puffing as a primary fuelling method. Gas puff will also be used on ITER combined with the pellet injection.

NBI injection: Neutral beam injection is a method used for heating tokamak (and stellarator) plasmas. Very energetic neutral particles are injected into the plasma column. These particles are usually deuterium atoms, therefore this heating method provides also deep plasma refuelling. However, attempting to refuel the plasma by NBI injection is very energy inefficient. The power required for sufficient refuelling rate is enormous.

Other possible fuelling methods include *gas blankets, plasma guns* or *cluster injection*. [7]

2.1 Pellet fuelling

With greater dimensions of the tokamaks, plasma refuelling by means of simple gas puffing would be inefficent, as the neutral gas particles would stay only on the plasma edge and would not be able to penetrate deeper into the plasma column. This is the reason why delivery of the fuel in the hotter, denser parts of plasma by pellet injection is inevitable for future devices to achieve the conditions for efficient controlled fusion. Pellet injection will also be crucial for ITER performance.

Solid pellets of frozen deuterium and tritium with diameters of 1-6 *mm* are used to refuel the plasma. Pellets are injected at high speeds (hundreds of meters per second) into the plasma column and they are able to reach the central plasma regions. The deep deposition of particles is beneficial and brings several advantages. Generally, it takes a longer time for a deeper delivered particles to escape out from the toroidal trap by a diffusive way, simply because of the longer distance it has to go, and therefore particle confinement time increases. In experiments undertaken at several toroidal devices, energy and particle confinement improvement has been observed associated also with greater thermonuclear reactivity. The pellet injection also allows us to operate at higher densities, both in L and H-mode regimes, and to better control the shape of the plasma density profile. The fuelling efficiency, defined as the proportion of the deposited material that remains effectively in the discharge, has been also observed to increase with the deeper pellet penetration.

2.1.1 Shielding

When injected into a hot plasma, surface of the pellet ablates, creating a large cloud of neutral gas, which can be up to 100 times larger than the pellet itself. The outer edge of this cloud interacts directly with plasma, is heated and ionized. The heat is then transported to the pellet and continues to ablate its surface. As the pellet gets deeper into the plasma column, its evaporation rate is increased. This neutral cloud of particles effectively protects the pellet from direct interaction with plasma particles and thus prolongs its lifetime and increases the pellet penetration depth. There are three main mechanisms of shielding provided by the neutral gas:

1) *Magnetic shielding:* Plasma at the outer edge of the gas cloud distorts local magnetic field, causes its partial expulsion from the cloud interior and thus reduces the incident heat flux. The rate of shielding by this phenomenon is almost negligible in present experiments.
2) *Electrostatic shielding:* The cold cloud may be charged negatively with respect to the hot background plasma. Therefore it accelerates the ions and repel the electrons. The thermal ions dissipate all their energy in outer layers of the ablation cloud and therefore the heat flux at the pellet surface is reduced.
3) *Gas dynamic shielding:* The neutral gas shields the surface of the pellet from direct interaction with flux of energetic plasma particles via collisions with these particles. For hydrogen pellets, this process is by far the most important. On this shielding phenomenon, the most widely used neutral gas shielding (NGS) model is based.

2.1.2 Fuelling efficiency

Fuelling efficiency of the pellet injection is relatively high. It can be in a range of 50-100%, which is much more than maximally a few percent efficiency of the gas puffing. It has been observed, that the main parameters, which influence the pellet penetration depth and consequently also the fuelling efficiency, are the pellet size, injection velocity and also the trajectory. Performed experiments confirmed, that injection of the pellets from the magnetic high field side (HFS) leads to a more efficient fuelling and lower confinement degradation with additional power, despite a limited pellet velocity. This is due to gradB induced drift of the ablated material. The cloud of ablated material is displaced along the magnetic field gradient, leading to deeper penetration for pellets injected from the HFS compared to the pellet fuelling from the low field side (LFS). [8] [9]
Even a pellet acceleration towards the low field side was observed, in a range of $(1\text{-}5)\cdot10^{5}\ m\cdot s^{-2}$, which can be explained also as the effect of gradB drift. Due to the gradB drift, a part of the shielding cloud drifts towards LFS and thus causes reduced pellet shielding at HFS compared to its LFS. Increased ablation at the HFS of pellet causes pellet rocket acceleration. [10]

2.1.3 Pellet production, acceleration, injection

Solid hydrogen pellets may be produced by two methods:

1) Hydrogen gas condenses and solidifies in a small part of narrow tube and then is ejected by high presure gas (MAST)
2) Hydrogen gas is liquified an then pushed through the extruder where it solidifies and then is cut mechanically. (JET).

For pellet acceleration, a variety of ways have been considered, I will mention the main ones:

1) *Electromagnetic:* Electromagnetic accelerators have been proposed to accelerate a carrier holding the pellet. The pellet will then enter the plasma and the carrier will be caught.
2) *Ablation:* A laser or electron beam incident on one side of the pellet would ablate away a part of its surface and thus accelerate the pellet by a rocket effect. This acceleration must be done gradually to avoid fracturing the pellet by shock waves.
3) *Centrifuge:* The pellet may be accelerated by placing it into a rotating arm. The pellet velocity achievable by this way is limited by the arm and pellet strength to velocities less than 5 $km \cdot s^{-1}$. This is for example the way of accelerating the pellets on JET.
4) *Light gas guns:* With solid hydrogen, velocities of 1 $km \cdot s^{-1}$ have been achieved. However, it is difficult for these guns to attain high repetition rates. [7]

The accelerated pellet than travels through a flight tube and is injected into the plasma. In order to access the vacuum vessel, especially from the HFS, the flight tube need to be curved. The curvature radius then determines the maximal possible pellet velocity (because of the stress experienced by the pellet in curved sections). This is an issue also for ITER. It will be difficult to generate strongly peaked density profiles on ITER because velocities of several kilometers per second are needed for a penetration depth up to 0.3 *a*. The ITER pellet injection system will be limited by a flight tube radius of 0.9 *m* to velocity of 300 $m \cdot s^{-1}$ from the HFS. [11]

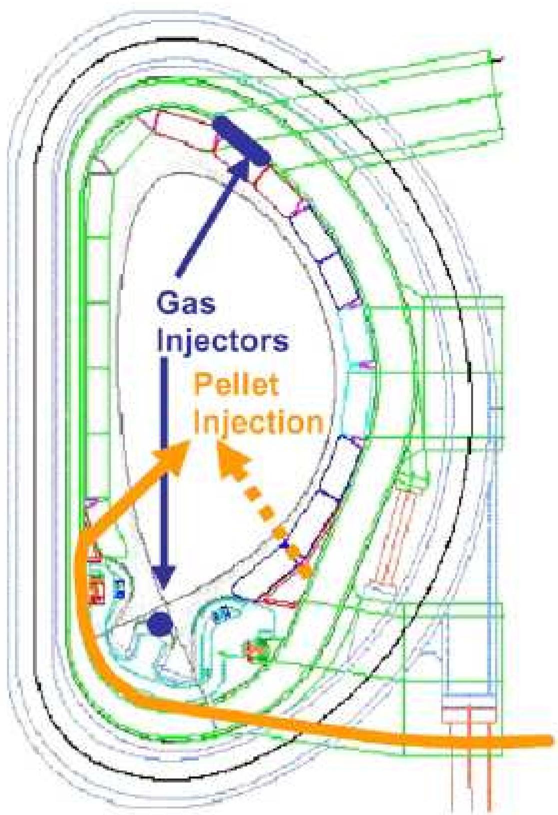

Figure 2.1: ITER cross section showing the locations of pellet and gas injectors. The dashed pellet trajectory shows proposed LFS pellet injectors intended for ELM triggering. [11]

There are also other functions which may be performed by the injection of pellets. Recently the pellets are studied for their capability of ELM mitigation. Edge localised modes (ELMs) are MHD instabilities in the pedestal region typical for H-mode scenarios. They provide outbursts of energy and particles from the plasma in a quasi-periodic way. They are followed by a phase of pedestal pressure rebuilding. Pellets tend to trigger ELMs automatically. These pellet induced ELMs are responsible for a significant loss of the deposited material, however, it can be used to our benefit. It has been shown, that increasing the ELM frequency by external pacemaking using pellet injection results in a reduced ELM energy, which is essential for the target lifetime of ITER and a future fusion reactor. [12]

Another function, which may be peformed by the pellet injection system in future fusion reactors is fast plasma termination. This function will be required in future fusion reactors, beacuse in a case of loss of control of the plasma equilibrium at high performance, the damage caused to first wall materials could be too high. One of the possible ways for mitigation of the plasma disruption is injection of a 'killer' – pellet of medium Z impurity. The pellet radiation would then decrease the plasma thermal energy and thus limit the heat flux onto the divertor plates.

One of the pellet injection advantages with respect to gas puff is also the possibility of decoupling the edge and core plasma parameters, mainly the possibility to increase the core density without changing the edge density.

For this chapter I have been using following materials: [3] [4] [7] [8] [9] [10] [11] [12], where you can find more detailed and complete analysis of the pellet refuelling, especially in [8].

3 Experimental results

I have been evaluating data from the JET pulse 53212. The basic parameters of this discharge are summarized in Tab.3.1:

Plasma current I_p	*2.5 MA*
Toroidal magnetic field B_t	*2.4 T*
Major radius R	*2.96 m*
Minor radius a	*0.92 m*
Elongation κ	*1.7*
Edge safety factor q_{95}	*3.2*
Plasma volume V_p	*80 m^3*
Plasma averaged triangularity $<\delta>$	*0.34*
Additional plasma heating P_i	*17 MW NBI, 1 MW ICRH*

Table.3.1: Summary of basic parameters of JET pulse number 53212

This pulse was a part of experiments undertaken at JET aimed to develop optimized pellet refuelling scenarios. Pellet injection sequences were optimized for long pulse fuelling to high densities near the Greenwald density while maintaining the H-mode and good energy confinement and keeping the impurity level low. These experiments also tried to combine positive effects of deep pellet refuelling and high plasma triangularity.

The present JET pellet injection system is able to produce approximately 4 mm^3 cubic deuterium pellets containing roughly $3 \cdot 10^{21}$ atoms and deliver them into the plasma at a maximum repetition rate of 10 *Hz*. Pellet size, velocity and repetition rate are fixed within one plasma discharge. However, repetition rate can be reduced by omitting single pellets. Pellets are launched at speed 160 $m \cdot s^{-1}$ from the HFS along a determined trajectory tilted by 44° to the horizontal plane.

For this pulse, there were three sequences of pellets injected into the plasma column – sequence of five, six and six pellets. The first sequence starts at time t = 57.87 s, pellets injected at a preset repetition rate of approximately 6Hz. Then two single pellets are omitted and the next sequence of six pellets is injected at time t = 58.98 *s* at halved repetition rate of approximately 3 *Hz*. Then three single pellets are omitted before the last pellet injection sequence starts at t = 61.22 *s* also with reduced repetition rate of approximately 3 *Hz*.

I downloaded the following data:

1. Line averaged plasma densities at multiple times measured by interferometer along 8 different lines (see Fig.3.1)
2. Electron density profiles at multiple times measured by LIDAR laser beam (see Fig.3.1).
3. Electron temperature profiles at multiple times measured by the same diagnostics as above.
4. D_α emisson measured by visible spectroscopy.
5. Total plasma energy content W_{dia} measured by two diamagnetic coils.

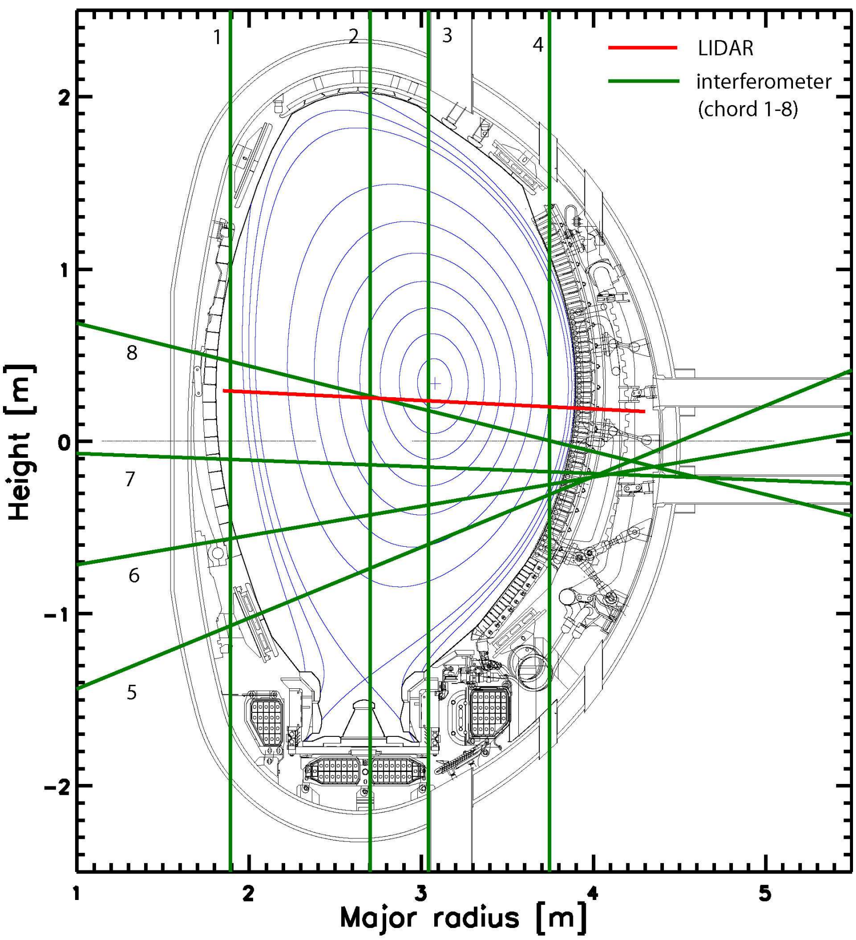

Figure 3.1: Plasma poloidal cross section with shown trajectories of LIDAR laser beam (red) and 8 chords of interferometer (green). Blue lines show the magnetic surfaces.

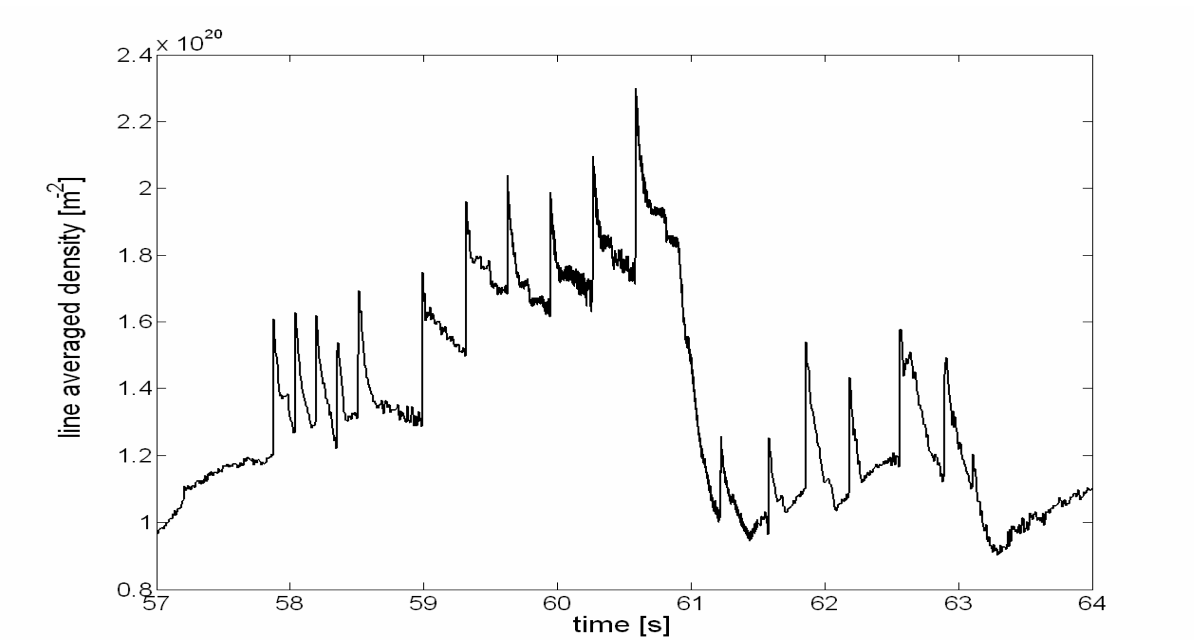

Figure 3.2: Line averaged plasma density measured by chord 8 of interferometer for the times of the three pellet sequences.

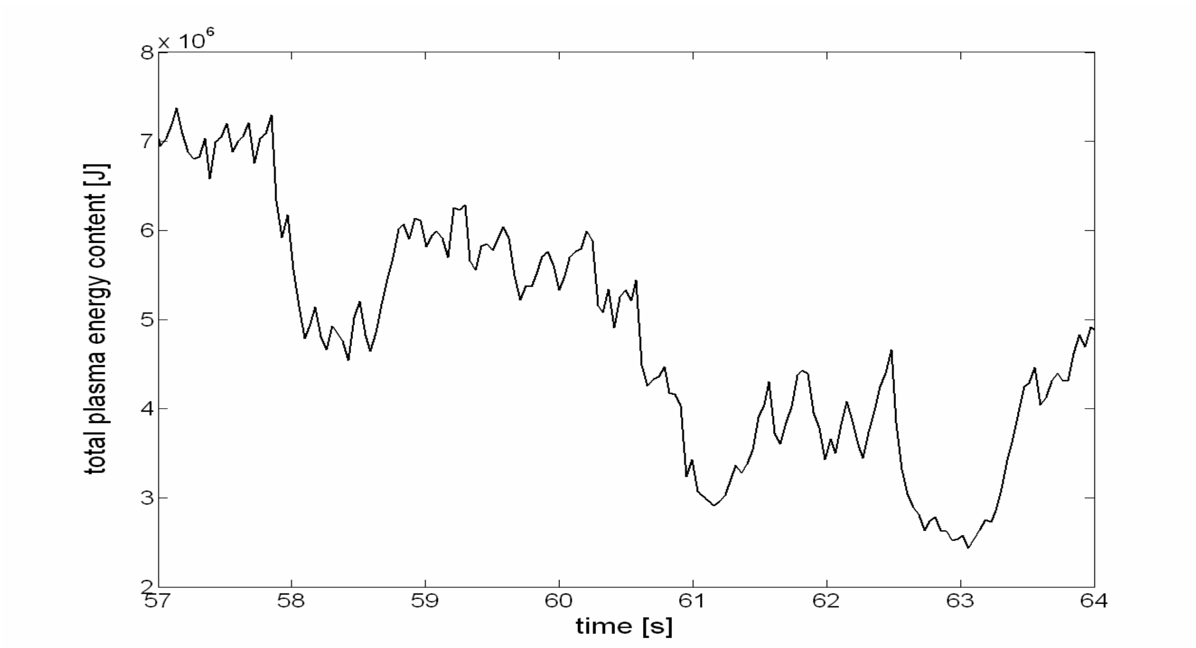

Figure 3.3: Total plasma energy content in joules for the times of the three pellet sequences.

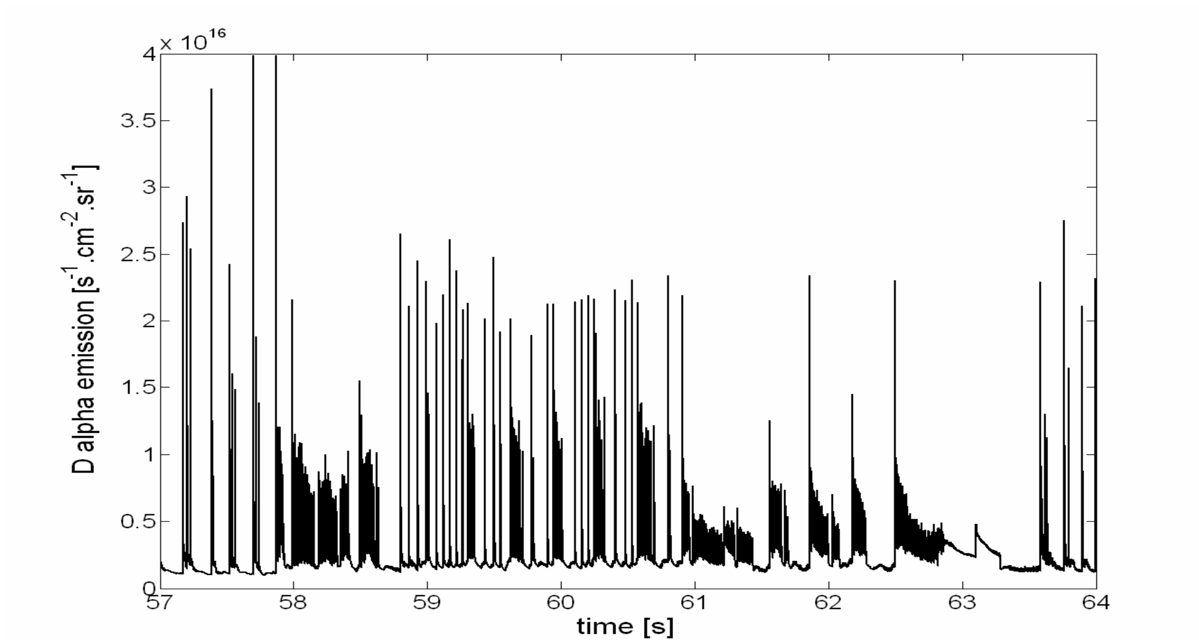

Figure 3.4: D_α emission for the times of the three pellet sequences.

3.1 Plasma response to the pellet

As was previously mentioned, the main intention of the series of pellet experiments at JET including pulse 53212 was to access densities in the vicinity of Greenwald density n_e^{Gw} (Greenwald density is an experimentally determined limit of plasma density), while keeping the confined energy high. During these experiments several critical issues appeared:

- Excessive increase of the plasma edge density

- Trigger of central MHD activity
- ELM bursts following pellet injection

Each of these effects connected with pellet injection can cause severe energy losses and therefore attempts were made to minimize them.

The excessive increase of the edge density could be limited by lowering the maximum pellet injection rate to 6 *Hz*. The pellet induced increase of neutral gas pressure then did not reach such high values to be able to deteriorate the confinement. The MHD activity, namely so-called neoclassical tearing mode (NTM), triggered by temperature reduction due to pellet, could be avoided by increasing the external plasma heating. Confinement losses caused by enhanced ELM activity were reduced by adapting the pellet injection cycle. Omiting single pellets leads to reduction of ELM activity and consequently to recovery of the plasma energy content.

As you can see on Fig.3.2, the averaged electron density strongly increases for a short time after each pellet injection, reaches its maximum and then drops down again, until the next pellet is injected. The first short phase of strong density increase describes the pellet evaporation. The outer atoms of the pellet ablate in the hot plasma and are ionized. The moment of total pellet evaporation can be seen on Fig.3.2 as the time of local maximum of density. The prompt post pellet particle losses can be explained by transiently increased plasma radial diffusivity because of increased density gradient. Also pellet induced ELMs may carry out immediately a very large fraction of the pellet delivered particles.

The frozen pellets injected into the plasma column accordingly decrease the plasma temperature. As will be mentioned later, this decrease is proportional to density increase and product of plasma density and temperature remains approximately the same during the pellet injection. Injection of each pellet also results in quick energy loss, mainly due to a triggered ELM. However, in phases between the injected pellets and especially in longer periods between two pellet sequences, the energy manages to recover.

Evolutions of essential plasma parameters for the described JET pulse are shown on Fig.3.2-3.4. We can clearly observe that initial quick 6 *Hz* pellet sequence caused significant energy drop due to enhanced ELM activity (which can be identified from increased intensity of D_α emission). To allow the energy to recover, two pellets were omitted before the onset of second pellet injection. The first pellet sequence including the following pause transformed plasma to a higher density state and was able to maintain the energy content still high. The second pellet sequence at halved repetition rate of 3 *H*z was able to achieve even better refuelling performance. This could be caused by the fact, that colder and denser plasmas are more suitable for deep particle deposition. The low injection rate also enabled the energy, which transiently drops after each injected pellet, to be almost fully recovered before injection of the next pellet. Therefore the plasma density was able to surpass the Greenwald level with about 6.1 *MJ* energy content. Finally, this high performance phase was terminated by a growing NTM. The next pellet sequence then starts from a low density level with low confined energy and is not able to achieve the previous high confinement level. [4]

3.2 Pellet size

The pellet size can be estimated from the increase of electron density profile during the pellet evaporation phase. For my calculations I used two consecutive density profiles measured by LIDAR in times t = 57.63 s and t = 57.88 s around the first injected pellet. The first profile shows the plasma density before the first pellet, the second one almost exactly in the moment of its total evaporation, therefore I was able to approximately determine the number of particles contained in single pellet from the difference of these two profiles.

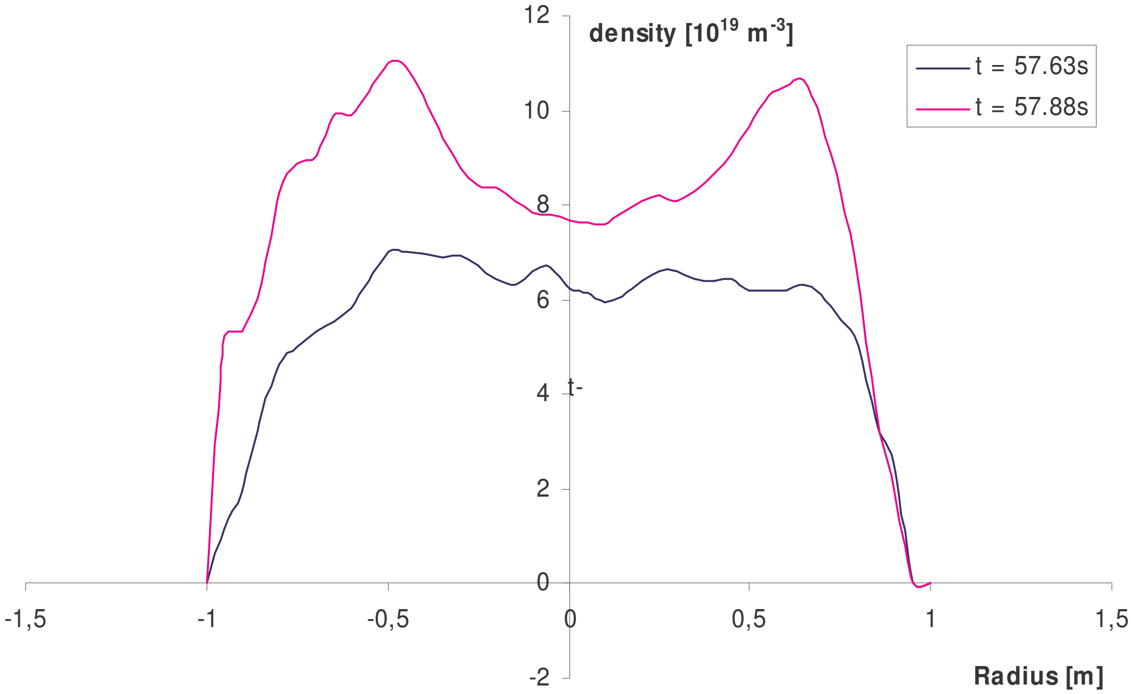

Figure 3.5: Two consecutive density profiles in times 57.63 s and 57.88 s.

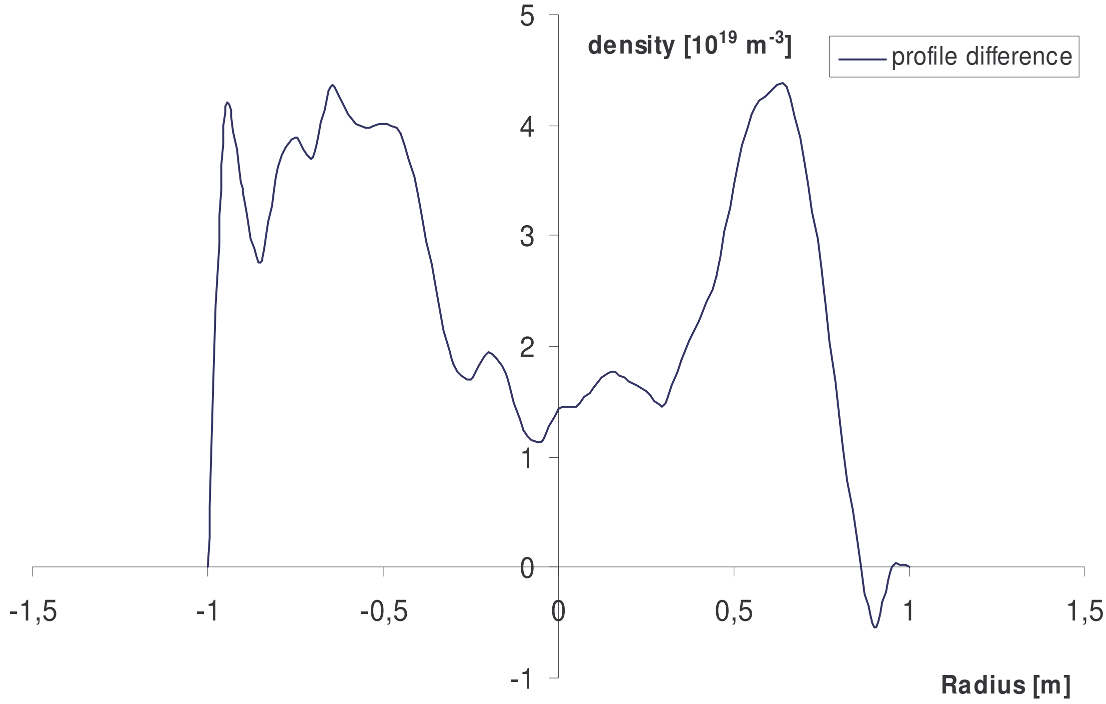

Figure 3.6: Difference of the two mentioned density profiles

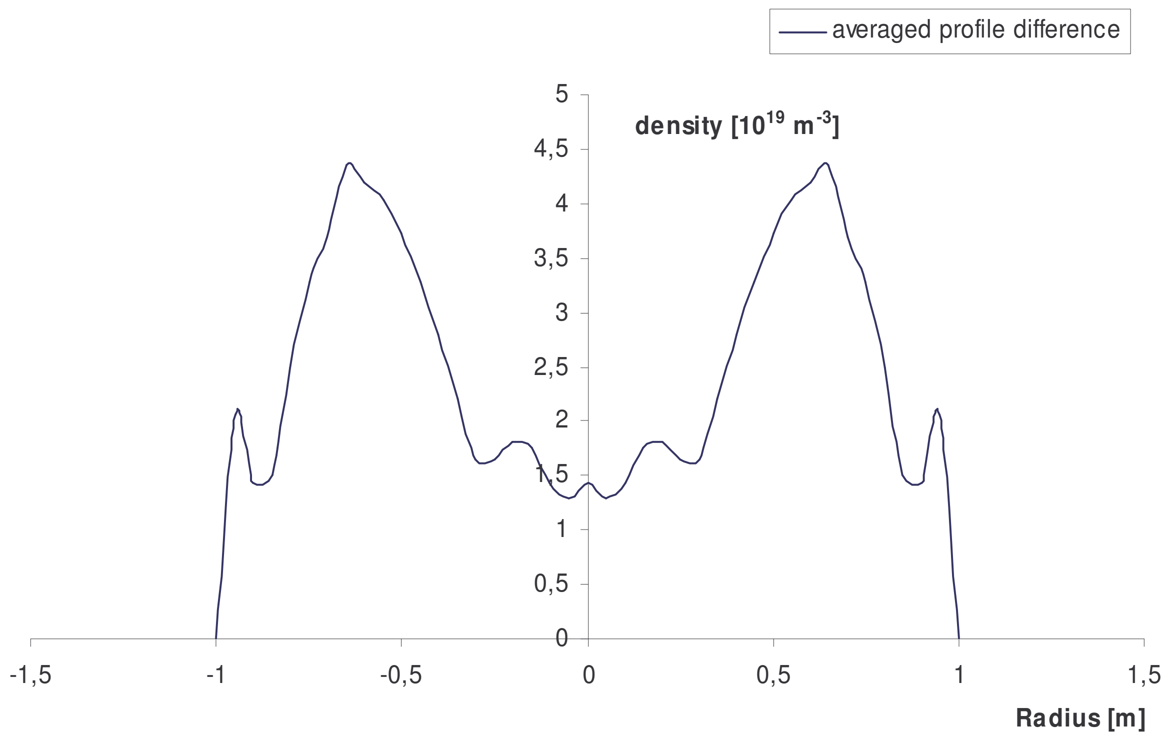

Figure 3.7: Averaged difference of the two mentioned density profiles
in order to gain even function

The plasma density is a function of time and position, $n = n(\vec{r}, t)$. Assuming this function can be factorized to a product of separate functions of time and position, $n = n(\vec{r}) \cdot n(t)$, I am able to exclude the time dependance. As we can see on Fig.3.2, plasma averaged density before the first pellet changes slowly in time and is almost constant, therefore I assume the time dependance to be constant during the short evaporation phase (less than 0.01 *s*). Another simplification of the density dependance can be made because of the toroidal plasma symmetry. The plasma parameters does not differ much in the toroidal direction and I am able to declare them constant in this direction. After accepting these conditions I am able to write the density only as a function of two coordinates lying in the poloidal plasma cross-section, $n = n(x, y)$. LIDAR on JET measures density profile along a line, which is almost horizontal, leading near the plasma central region (Fig.3.1). For my calculations I need to know the density distribution on the whole plasma poloidal cross-section. Therefore I consider the plasma shape as elliptic and neglect its triangularity and also shape deformation in the divertor region. Then under a premise that the plasma density changes from the centre to the edge of plasma in a same way in all directions (it is constant on the magnetic surfaces), I am able to determine the values of density on the whole ellipse. However, under the terms of this premise I must modify the downloaded density profile to be an even function, which I performed by averaging the values belonging to places equally distanced from the minor axis. (Fig.3.7)

Total number of deuterium atoms contained in the pellet can be calculated from the following integral:

$$N = \int_V \Delta n(V) \cdot dV \,, \tag{3.1}$$

where Δn is the difference between density profiles before pellet injection and in the moment of total evaporation and V is the plasma volume. If I follow the simplifications mentioned above, I am able to write:

$$N = 2\pi R_0 \int_S \Delta n(x, y) \cdot dxdy \qquad \Delta n(x, y) = \Delta n(\frac{R}{R_\varphi} \cdot a, 0) \,, \qquad (3.2)\ (3.3)$$

where R_0 is the plasma major radius, S is the surface of the plasma cross-section, x and y surface cartesian coordinates, R distance from the minor axis, R_φ distance from the minor axis to the edge of ellipse for certain angle φ between the horizontal x-axis and positional vector $\vec{R}$ and a is the plasma minor radius, which is the same as the elliptic semiminor axis. After modification of the integral:

$$N = 2\pi R_0 \int_S \Delta n(\frac{\sqrt{a^2 y^2 + b^2 x^2}}{b}, 0) \cdot dxdy \,, \tag{3.4}$$

where b is the elliptic semimajor axis, it is advantageous to pass over from cartesian to elliptic coordinates (x,y)→(σ,φ) by an elliptic transformation Φ:

$$x = a \cdot \sigma \cdot \cos\varphi \qquad \qquad |J_\phi| = a \cdot b \cdot \sigma \,, \qquad (3.5)\ (3.6)$$
$$y = b \cdot \sigma \cdot \sin\varphi$$

where $\sigma \in \langle 0,1 \rangle$, $\varphi \in \langle -\pi, \pi \rangle$ and $|J_\phi|$ is the Jacobian determinant of the transformation. The resultant integral is then after a further simple substitution in the following form:

$$N = 4\pi^2 R_0 \cdot \kappa \cdot \int_0^a n(w) \cdot w \cdot dw \,, \tag{3.7}$$

where $\kappa = \dfrac{b}{a}$ is elongation and w is an artificial variable. The integral must be evaluated numerically, as area below the graph on Fig.3.8.

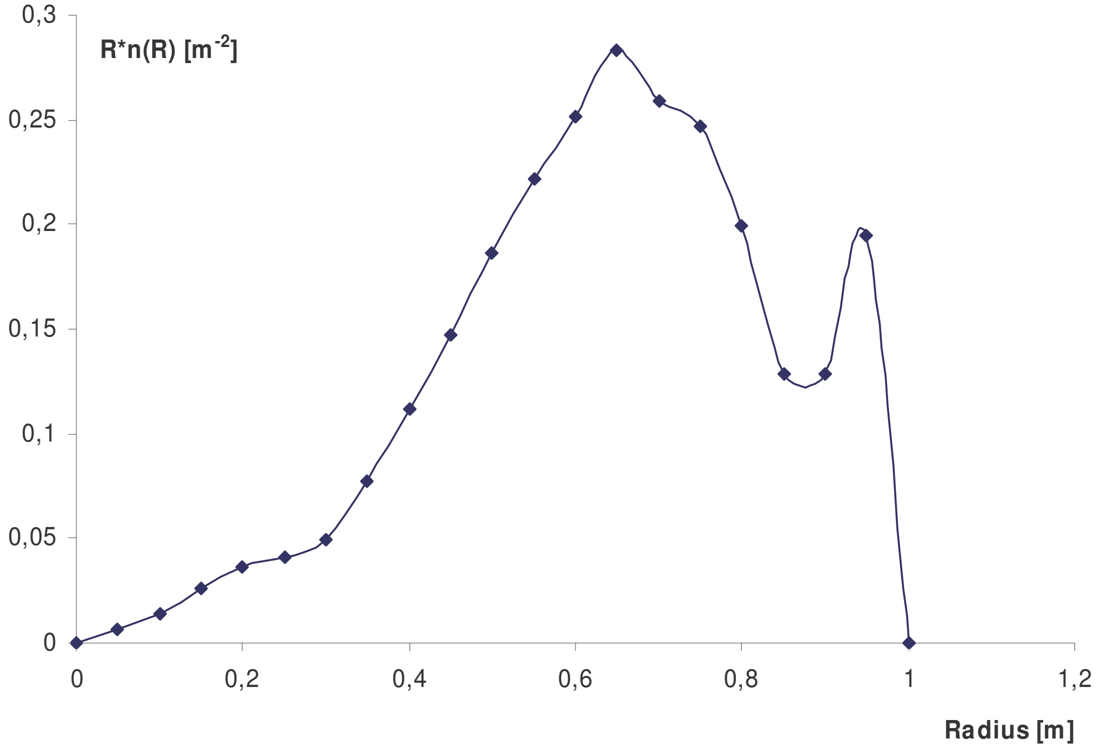

Figure 3.8: Graph of the function in integral (7), the area below the graph is the value of integral.

The value of the integral is $S = 1.304945 \cdot 10^{19}\ m^{-1}$, elongation $\kappa = 1.7$ and JET tokamak major radius $R_0 = 2.96\ m$. Therefore the computed number of particles contained in single pellet is $\boldsymbol{N = 2.59 \cdot 10^{21}}$. This numbered roughly corresponds to the expected value of $3 \cdot 10^{21}$ deuterium atoms quoted in the paper [4].

The assumption that plasma density is constant along the magnetic surfaces (in our assumption elliptical) is very common in tokamaks. The true quantity which is constant on magnetic surfaces is the total plasma pressure including the energy of plasma rotation. This follows from the Shafranov equation valid in MHD equilibrium. Due to the large parallel thermal conductivity along the magnetic field lines the electron and ion temperatures are also constant along the magnetic surfaces. Because plasma pressure can be calculated as:

$$p = n_e \cdot T_e + n_i \cdot T_i \approx n_e \cdot (T_e + T_i), \tag{3.8}$$

this means that also the electron density is approximately constant on magnetic surfaces.

The difference of 12% between our calculated pellet size and expected value is extremely good. The difference can be easily attributed to:

1. the losses of particles from the plasma between the two measurement times
2. the imperfection of measurement of the pellet size
3. losses in flight tube between the measurement point and the plasma

3.3 Adiabaticity of the plasma response to the pellet injection

In this part of this work I tried to determine, whether the plasma response to pellet is adiabatic. Adiabatic process is a thermodynamic process, in which no heat is transferred to and from the working system. For an ideal gas, it can be expressed mathematically as:

$$p \cdot V^{\frac{C_p}{C_V}} = const., \tag{3.9}$$

where p is ideal gas pressure, V is its volume, C_p is the specific heat for constant pressure and C_V is the specific heat for constant volume. For an ideal plasma, the potential energy of particles is negligible compared with their kinetic energy and the plasma is weakly coupled. Such plasma is therefore similar to gas and sometimes we refer to it as ionized gas. The ideal gas equation of state is then a good approximation of the plasma particles equation of state. If we assume the JET plasma to be weakly coupled, then we are able to describe it by the ideal gas equations. The plasma coupling can be described by the coupling parameter Γ:

$$\Gamma = \left(\frac{4\pi}{3}\right)^{\frac{1}{3}} \cdot \frac{Z^2 e^2 n_i^{1/3}}{k_B T_i}, \tag{3.10}$$

where Z is the charge carried by plasma ions, e is the charge of an electron, n_i is the ion density, k_B is the Boltzmann constant and T_i is the ion temperature. [13] For JET and all magnetic fusion plasmas $\Gamma << 1$, therefore our assumption is correct. We may now use the following equations:

$$p \cdot V = N \cdot k \cdot T \qquad p = \frac{N}{V} \cdot k \cdot T = n \cdot k \cdot T, \qquad (3.11)\ (3.12)$$

where the equation (3.12) is the equation of state, N is the number of particles contained in volume V, T is temperature and n is density (number of particles per volume). The tokamak plasma volume remains constant during the discharge, therefore processes in the plasma are adiabatic, if the following equation is accomplished:

$$p \approx n_e \cdot (T_e + T_i) = const., \tag{3.13}$$

Where the total pressure is the sum of ion and electron contributions. It should also be noted that no process is really adiabatic. Many processes are close to the adiabatic process and can be approximated by using an adiabatic assumption, but they always have a heat loss.

In order to determine, whether the pellet evaporation processes are adiabatic, I have chosen two pressure profiles in times t = 57.63 s and t = 57.88 s. Other profiles were not so suitable, because they include plasma energy losses between the single pellets, mainly due to ELMs.

The first considered profile is before the injection of the first pellet and the second profile is in time of the total pellet evaporation. For the evaluation of plasma pressure I used the equation (3.13) and I made an assumption, that the plasma ion temperature is equal to the plasma electron temperature:

$$T_i = T_e \tag{3.14}$$

The two plasma electron pressure, electron temperature and electron density profiles in times discussed above are given on Fig.3.9-3.11.

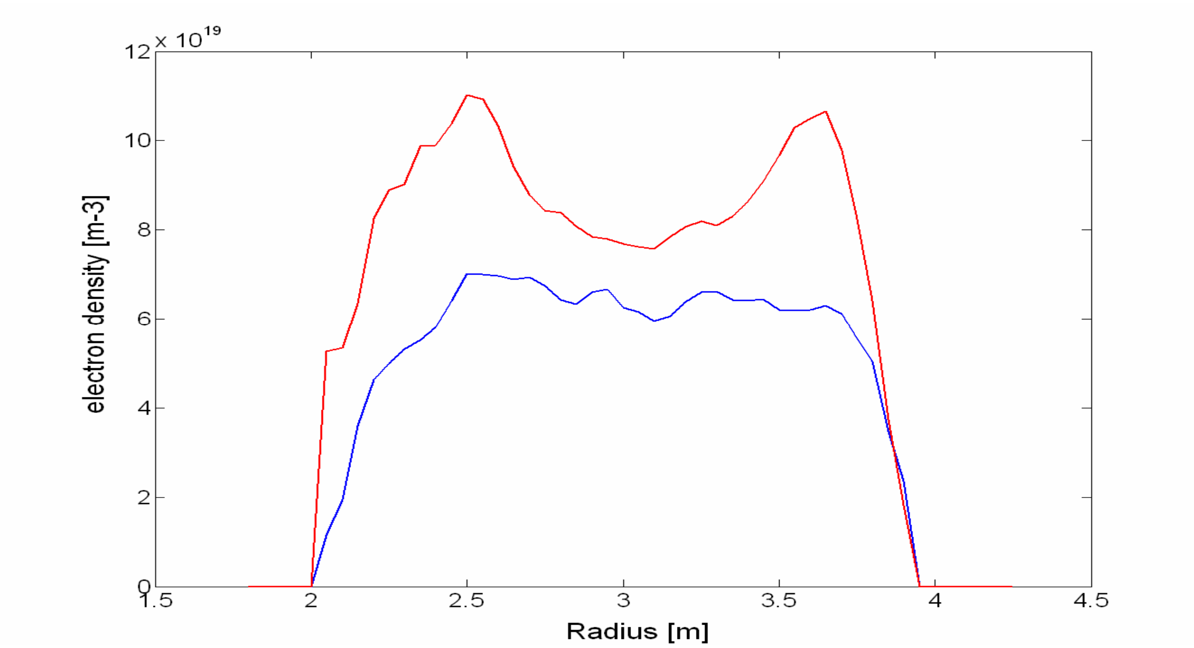

Figure 3.9: Two profiles of plasma electron density in times $t = 57.63$ s (blue) and $t = 57.88$ s (red).

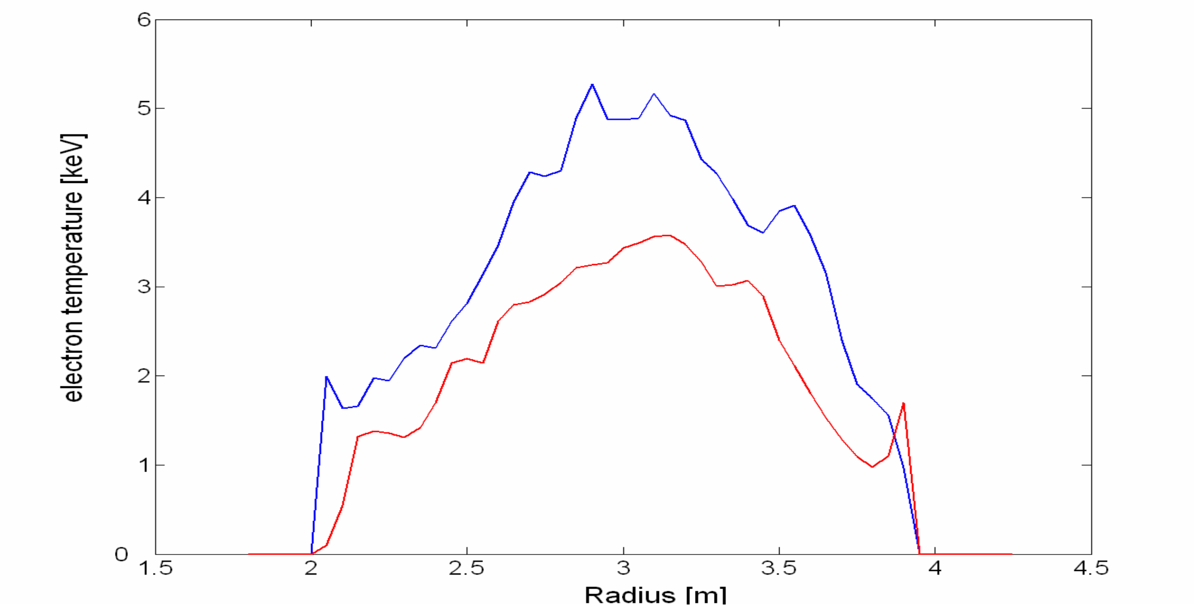

Figure 3.10: Two profiles of plasma electron temperature in times $t = 57.63$ s (blue) and $t = 57.88$ s (red).

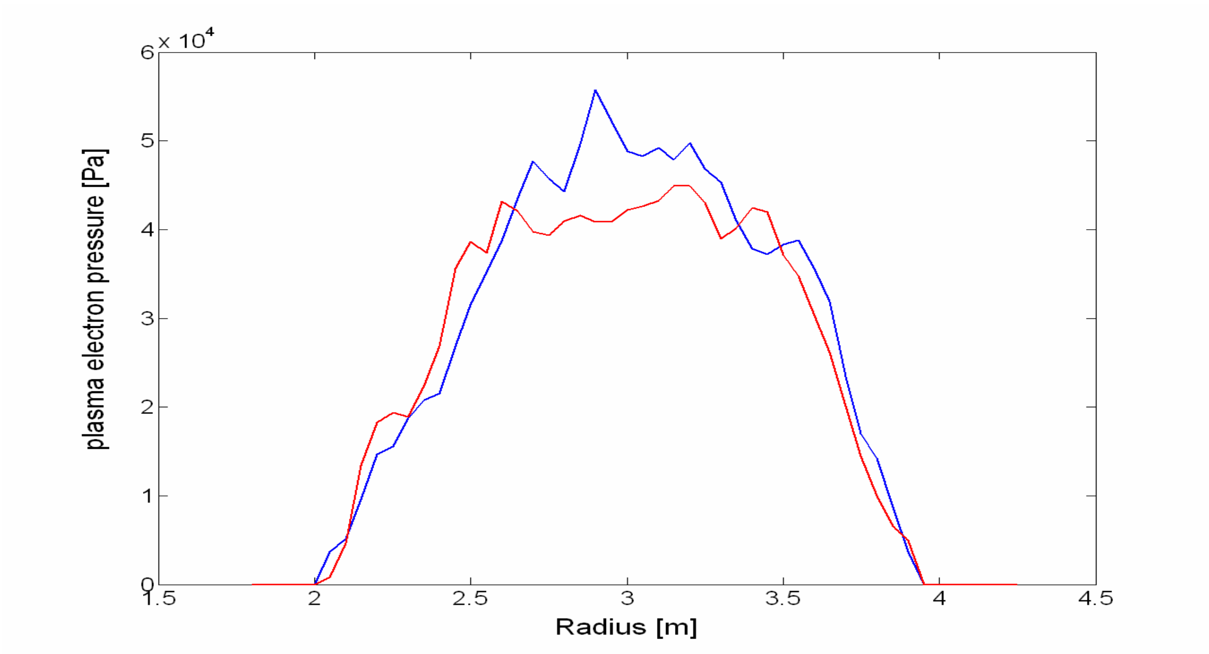

Figure 3.11: Two profiles of plasma electron pressure in times $t = 57.63\ s$ (blue) and $t = 57.88\ s$ (red).

As we can see, that while the density and temperature profiles are different, the two pressure profiles are very similar, in particular in the zone of pellet deposition, where the density perturbation is maximum. Therefore it is possible to consider the plasma processes during the evaporation of the first pellet as approximately adiabatic. This is also supported by the fact, that no drastic changes occurred to the plasma total energy content. There was only a slight energy drop of approximately 11% between these profiles.

Finally, note that the adiabacity of pellet deposition is not exact. A part of plasma energy is consumed for evaporation and ionization of pellet, however this is small compared to the energy of plasma particles. Secondly, even during pellet evaporation and ionization process lasting few milliseconds, fast losses of plasma energy can occur. One of the examples is the pellet-triggered ELM which lasts few hundred microseconds. The approximate adiabacity shows that contributions of such processes are small in our case.

3.4 Particle transport

For a single particle in tokamak the confinement would be perfect. However, in reality collisions, drifts, MHD instabilities and turbulence lead to a radial transport of particles and energy. This radial transport determines the particle and energy confinement times τ_p and τ_E and therefore it is one of the most important plasma parameters.

We define the particle flux Γ as the number of particles passing through a magnetic surface per unit area and time. For Γ the following ansatz is made:

$$\Gamma = -D\nabla n + n \cdot v \, , \tag{3.15}$$

which says that it has a diffusive part driven by a density gradient and characterized by the diffusion coefficient *D* and a convective part due to directed motion *v*.

The equation of continuity says, that a change of density in any part of the system is due to inflow and outflow of material into and out of that part of the system, no material is created or destroyed. Mathematically expressed:

$$\frac{dN}{dt} = -\oint_S \Gamma dS \, , \tag{3.16}$$

where *N* is a number of particles contained in the system and *S* is an enclosed surface encircling the system. We are able to further modify this equation by using the Gauss's law :

$$N = \int_V n \cdot dV \qquad\qquad \oint_S \Gamma dS = \int_V (\nabla \cdot \Gamma) dV \qquad (3.17)\ (3.18)$$

where *V* is a volume enclosed by the surface *S*. Therefore we can write the resulting equation in a differential form:

$$\frac{\partial n}{\partial t} = -\nabla \cdot \Gamma \tag{3.19}$$

In reality, this equation contains an additional term, which describes the change of plasma density due to ionisation or recombination *S*:

$$\frac{\partial n(r,t)}{\partial t} = -\nabla \cdot \Gamma + S(r,t) \tag{3.20}$$

If we put the equations (3.15) and (3.20) together, we gain the final equation:

$$\frac{\partial n}{\partial t} = \nabla \cdot (D\nabla n) + \nabla \cdot (n \cdot v) + S \tag{3.21}$$

3.5 Diffusion coefficient

In a magnetized plasma we distinguish between transport coefficients parallel and perpendicular to the magnetic field. Diffusion parallel to the magnetic field lines is unaffected by the magnetic field and is generally much bigger than the perpendicular diffusion. The magnetic confinement properties, however, are determined by the perpendicular diffusion coefficient.

The simplest way of computing the diffusion coefficient comes from the random-walk assumption. We assume that due to Coulombic collisions with other particles, the particle makes a step Δx perpendicular to the magnetic field after a time Δt. The step can be made in both directions with equal probability and the diffusion coefficient is the following:

$$D \approx \frac{\Delta x^2}{2\Delta t} \tag{3.22}$$

To get the diffusion coefficient, it is necessary to evaluate the Δx and Δt. Δt is an average time which it takes for a particle to change its direction due to collisions by 90°. It is the inverse value of the collision frequency ν_e and it differs for electron-electron (ee), ion-electron (ie), electron-ion (ei) and ion-ion collisions (ii). For ion-electron collisions, we have got:

$$\nu_{ie} = \left(\frac{m_e}{m_i}\right) \cdot \nu_{ee}\,, \tag{3.23}$$

$$\nu_{ee} \approx \nu_{ei} \propto \frac{ne^4}{\sqrt{m_e} T_e^{3/2}} \tag{3.24}$$

In the so-called *classical approach*, we take Δx to be the Larmor radius r_L.

The location *R* of the guiding centre of the gyro-orbit is following:

$$\vec{R} = \frac{\vec{p} \times \vec{B}}{q_C \cdot B^2}\,, \tag{3.25}$$

where $\vec{p}$ is the particle momentum, $\vec{B}$ is the magnetic field and q_C is the charge of the particle. In a collision, momentum balance requires equality of $\Delta p_a = -\Delta p_b$. Therefore for collisions of equally charged particles (ions-ions, electrons-electrons) $\Delta R_a = -\Delta R_b$ and these collisions do not contribute to particle transport (only to a heat transport), beacuse the particles change place only. This changes for electron-ion collisions. Therefore the diffusion is *ambipolar*, in a collision the electrons and ions make a step of equal length and direction:

$$D_{e,class} = \nu_{ei} \cdot r_{L,e}^2 = \nu_{ie} \cdot r_{L,i}^2 = D_{i,class} \tag{3.26}$$

However, experimentally determined diffusion coefficients are larger by a factor of approximately 10^5.

In a *neoclassical approach* to transport, we consider the effects of toroidal geometry. There are two main differences to classical transport theory:

- $|B|$ is not constant along a magnetic field line. Plasma particle which does not have sufficient ratio of $\frac{v_{par}}{v_{perp}}$, where v_{par} means parallel and v_{perp} perpendicular velocity to the magnetic field, will be reflected back. Therefore we distinguish between two types of particles: trapped and passing. The electrical conductivity of plasma is lowered in a neoclassical theory, because the trapped particles do not contribute to the toroidal current

- The gradB and curvature drifts cause that a trapped particle deviates from the magnetic surface and its orbit projected into a poloidal plane has a banana shape. These orbits are therefore called *banana orbits*.

The neoclassical effects can increase the diffusion coefficient by a factor of 10^2. But it still cannot explain the experimental results. The real transport is called *anomalous* and it is a result of turbulences in plasma. [6].

3.6 Boxcar method

The plasma diffusivity can be estimated from the evolution of the density profile after the pellet injection. I used the downloaded data from LIDAR (electron density profiles) and interferometer 8 (line averaged density).
Unfortunately, LIDAR diagnostics measures the density profiles with a low frequency of 4 *Hz*, therefore it is not possible to directly evaluate the changes in plasma density due to pellet injection. The pellets are injected with a repetition rate of 6 *Hz* or 3 *Hz* and so the LIDAR measurement gives us usually 1-2 profiles of density per pellet, which is not sufficient for our calculations. On the other hand, interferometer measures density with a relatively high repetition rate of approximately 133 *Hz*, however, these densities are line averaged and thus does not provide us with much needed information about the density profile. One way how to get a more detailed picture of the time evolution of single pellet (in the following text, by a pellet I mean the plasma density evolution due to pellet) along with desired density profiles in each time is to make a *boxcar analysis* of the LIDAR data on the whole pulse and create one "average pellet". The idea of the boxcar analysis is following:

- In this method we assume that every pellet is the same and its injection has always the same impact on plasma density evolution.
- The LIDAR measurement comes for every pellet in a different time of its evolution in plasma. For each measurement, we calculate its relative time to the moment of injection of the actual pellet.
- We put these measurements together into a graph, where the x-axis is the relative time of the pellet. This way we are able to create an average pellet with much more points than we actually have for each real pellet.

For my calculations, I have done the boxcar analysis of the first and third pellet sequence from the JET pulse 53212 (starting at times t = 57.87 *s* and t = 61.22 *s*), which contain approximately equally shaped pellets. It is shown on the following figures (Fig.3.12, Fig.3.13). On these figures the top red graph shows the density evolution measured by LIDAR for R = 3.6 *m* (distance from the major axis), the bottom graphs show line averaged density measured by 8 chords of interferometer. The point of intersection of the black vertical lines (in the times of LIDAR measurement) with the interferometer data shows us, in which part of the pellet-induced density evolution the LIDAR measurement is located.

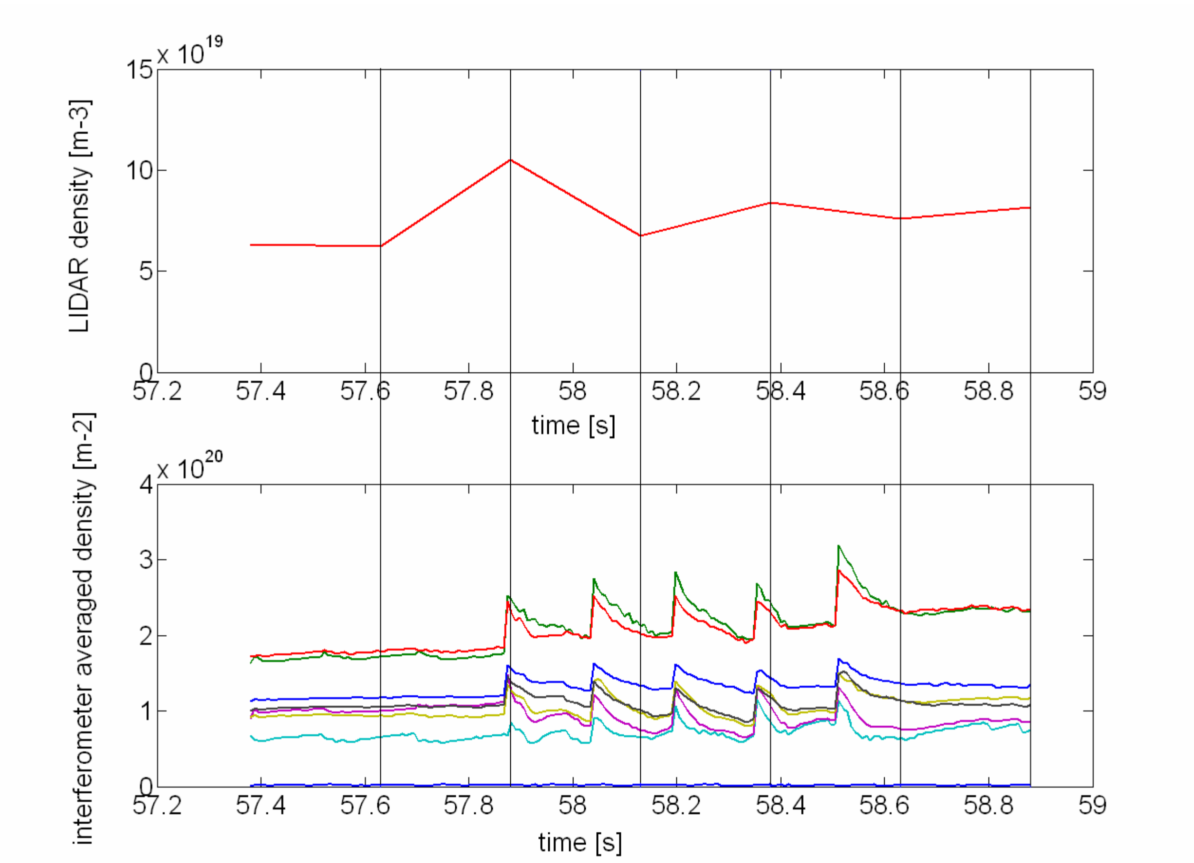

Figure 3.12: The boxcar analysis of the first sequence of pellets starting at $t = 57.87\ s$

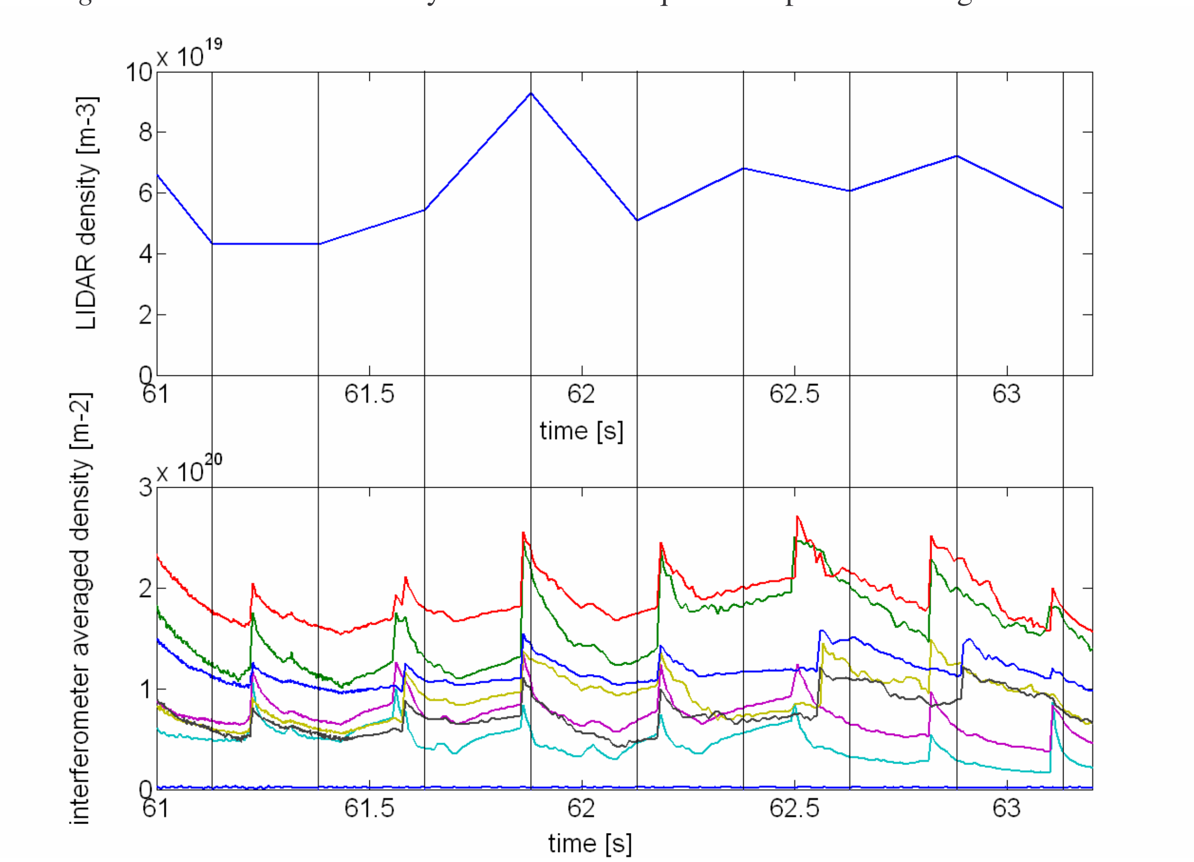

Figure 3.13: The boxcar analysis of the second sequence of pellets starting at $t = 61.22\ s$

From the downloaded interferometer data we are able to determine the pellet injection times (which correspond to the places with sudden strong increase of density) and with the aid of the figures above it is then possible to assign relative times to each LIDAR density measurement. This enables us to get the temporal evolution of line averaged density during the "average pellet". For the determination of pellet injection times, I used the eighth chord of interferometer.

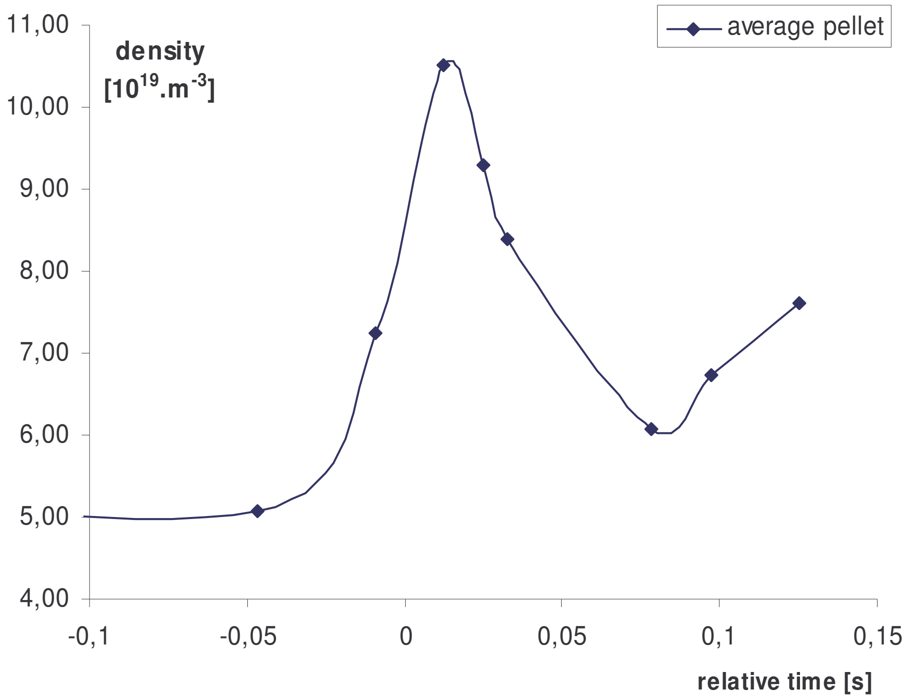

Figure 3.14: "Average pellet" - density evolution after the pellet injection (relative time = 0) for major radius R = 3,6 *m*.

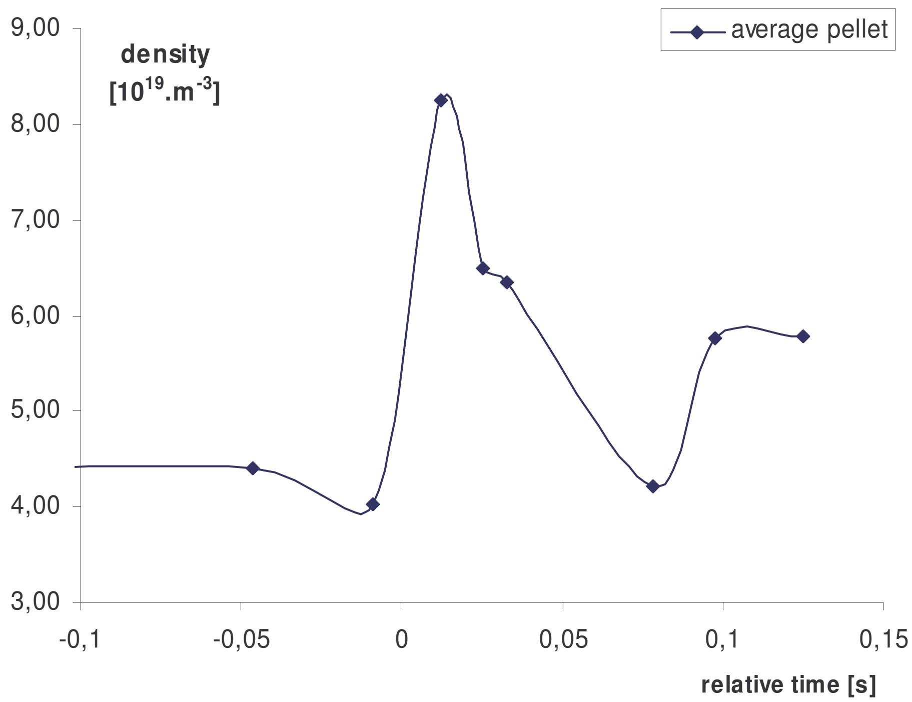

Figure 3.15: “Average pellet“ - density evolution after the pellet injection (relative time = 0) for major radius R = 3,75 *m*.

For illustration two graphs of the gained “average pellets“ at different radii are given (Fig.3.14, Fig.3.15). As you can see, average pellets gained by this method are not very precise, they only very crudely correspond to the real pellet shape, which we know from the interferometer data. This is caused by incorrect assumption about equality of the pellets made on the beggining of these calculations. Even though we tried to choose approximately the same pellets from the pellet sequences, the error of this method remains still high.

3.7 Evaluation of diffusion coefficient

For the calculation of the diffusion coefficient itself, I used a simplified version of diffusion equation (3.21):

$$\frac{\partial n(r,t)}{\partial t} = D \cdot \frac{\partial^2 n(r,t)}{\partial r^2}, \tag{3.27}$$

where I do not consider the ionisation source S, the convective transport and I assume the diffusion coefficient to be constant in space. It is very difficult to distinguish between diffusion and convection. Therefore so-called effective diffusion coefficient, which describes both these phenomena, is defined as:

$$\Gamma = -D_{eff} \cdot \nabla n \tag{3.28}$$

and the equation (3.26) can be written as:

$$\frac{\partial n}{\partial t} = \nabla \cdot \left(D_{eff} \nabla n \right) + S \tag{3.29}$$

In the following text by writing D I always mean effective diffusion coefficient D_{eff} and the computed diffusion coefficient is in fact effective diffusion coefficient. Calculation of S is also very difficult. It can be expressed as:

$$S = \nabla \cdot \Gamma_{ionisation}, \tag{3.30}$$

where $\Gamma_{ionisation}$ is the particle flux caused by the source S of particles due to ionisation or recombination. The equation (15) can then be written as:

$$\frac{\partial n}{\partial t} = \nabla \cdot \left(D \cdot \nabla n + \Gamma_{ionisation} \right) \tag{3.31}$$

According to [15], $\frac{\Gamma_{ionisation}}{n} \approx 0.5 m \cdot s^{-1}$ for $r/a = 0.8$. This value is approximately ten times lower than $D \cdot \frac{\nabla n}{n}$ and as a result we can neglect the contribution of S compared to the diffusion and convection terms.

For a numerical calculation of diffusion coefficient from discrete experimental data, I needed to approximate the derivatives by difference equations. I used the following simplifications:

$$\left(\frac{d^2 f(q)}{dq^2} \right)_{q_0} \approx \frac{f(q_0 + \Delta q) - 2f(q_0) + f(q_0 - \Delta q)}{(\Delta q)^2}, \left(\frac{df(q)}{dq} \right)_{q_0} \approx \frac{f(q_0 + \Delta q) - f(q_0)}{\Delta q}, \tag{3.32}$$

where f is differentiable universal function of a variable q, Δq is a small increment of the variable q and (q_0) is a point, in which the derivation is evaluated. Another possibility, not used in this work, is to fit the experimental data by continuous function and then calculate the derivatives of this function.

Using the equations (3.32) the diffusion equation (3.27) may be written in the following form:

$$\frac{n_e\left(\frac{R_1 + R_2}{2}, t_2 \right) - n_e\left(\frac{R_1 + R_2}{2}, t_1 \right)}{t_2 - t_1} = 4D \cdot \frac{n_e(R_2, t_1) - 2n_e\left(\frac{R_1 + R_2}{2}, t_1 \right) + n_e(R_1, t_1)}{(R_2 - R_1)^2}, \tag{3.33}$$

where (R_1,R_2) is interval of radii in which the main diffusive particle transport occurs (the gradient of density is the steepest), (t_1,t_2) is a time range in which the change of density is observed. The diffusion coefficient is then evaluated in the point $\left(\frac{R_1 + R_2}{2}, t_1 \right)$. The times t_1 and t_2 used for the calculation are taken from the evolution of the averaged pellet. On the figures of average pellets (Fig.3.14, Fig.3.15) you can clearly see, that only three time intervals from the desired part of the pellet are available (from the part of quick density drop due to enhanced particle transport after the pellet evaporation). The interval of radii used for the calculation may be gained from the following figure (Fig.3.16), which shows evolution of the density profile around the first injected pellet (t = 57.87 s). The blue line shows the density profile before the injection, green line shows the density profile almost exactly in the time of total evaporation and the red line shows the resulting peaked profile after the pellet. As we can see, the profile in the moment of total evaporation is hollow. The steep density gradient on the plasma edge determines the outward particle diffusion. It is located in interval of radii 3.65 - 3.95 *m* and therefore I used this interval for the calculaton of the diffusion coefficient.

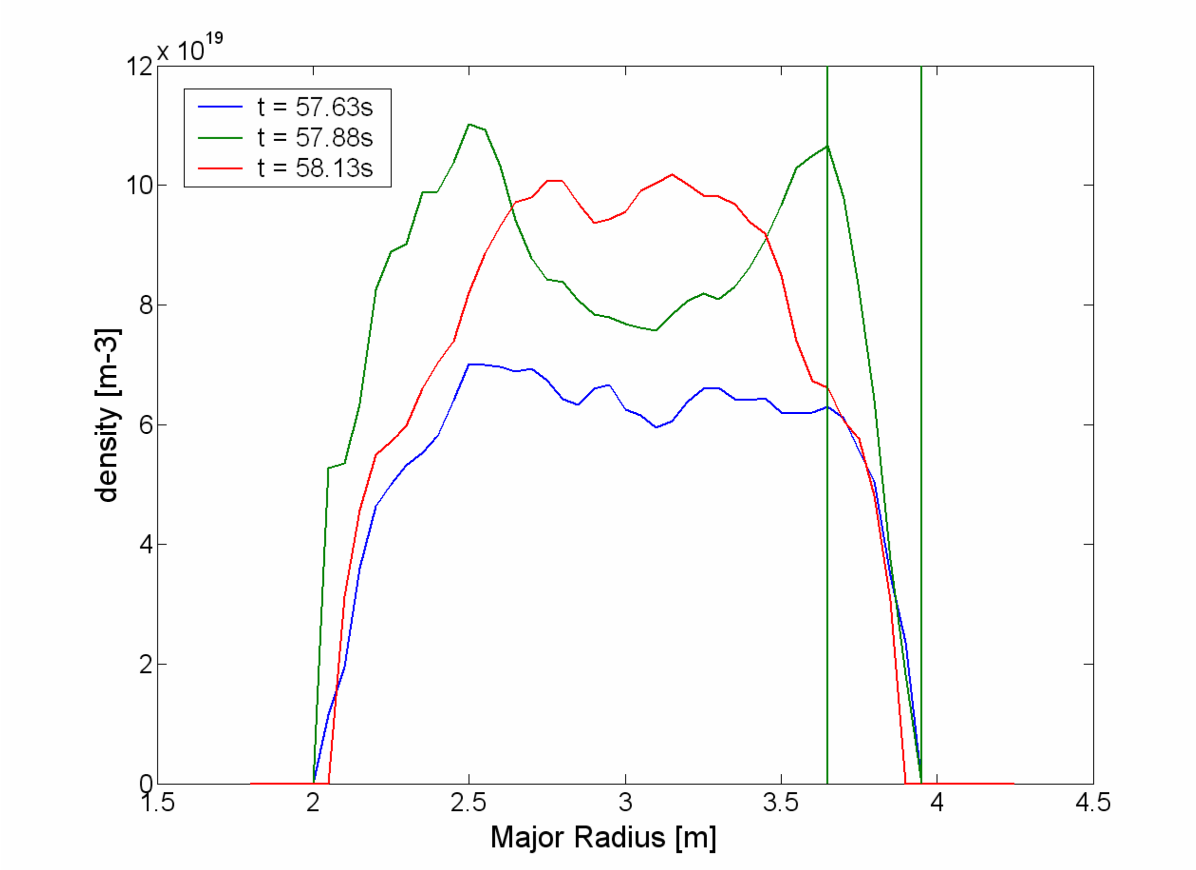

Figure 3.16: Evolution of the density profile around the time of the first pellet

After numerical evaluation of the equation (3.33) I obtained the following three values of the diffusion coefficient, corresponding to different times after the pellet:

- ***D = { 0.7589; 0.2899; 0.2974 } $m^2.s^{-1}$***.

In the next part of the work I evaluated the error of this calculated coefficient in order have more complex idea about its real value. The error of measured or calculated value of some quantity can be estimated from the following equations:

$$u = f(x, y, \ldots) \qquad \sigma_u = \sqrt{\left(\frac{\partial f}{\partial x}\right)_0^2 \sigma_x^2 + \left(\frac{\partial f}{\partial y}\right)_0^2 \sigma_y^2 + \ldots}\,, \qquad (3.34)\ (3.35)$$

where u is the calculated/measured quantity, (x, y,..) are the variables on which this quantity depends, which were measured/computed with some error $\sigma_{x,y,..}$, σ_u is the wanted error of the quantity u and 0 means the point (x_0, y_0,..) of the measured/computed values. In our case, after replacing the derivations by differences, the diffusion coefficient D is a function of four variables: $n_e((R_1+R_2)/2,t_1)$, $n_e((R_1+R_2)/2,t_2)$, $n_e(R_1,t_1)$ and $n_e(R_2,t_1)$. The measurement of the density profiles by LIDAR features a certain error, which is given with the density profile measurement values. On Fig.3.17 you can see an example of density measurement error for time t = 57.88 s.

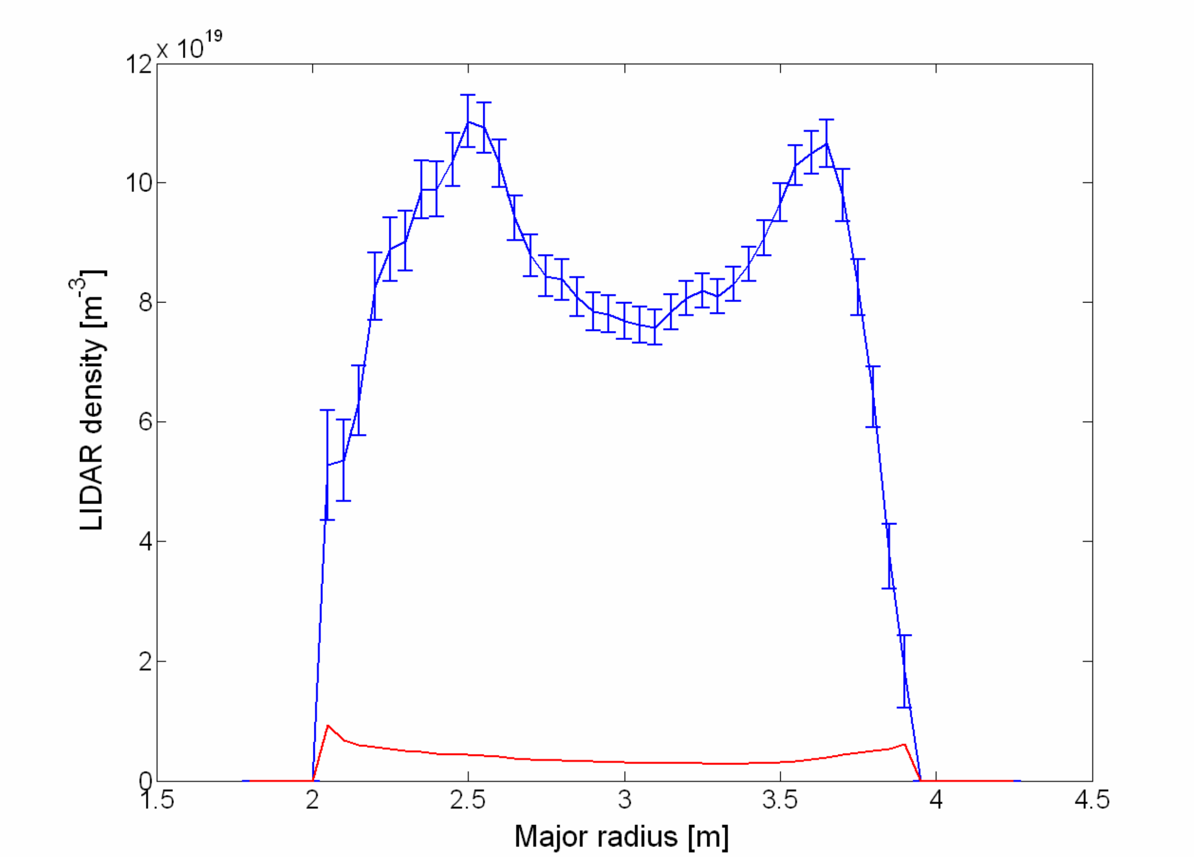

Figure 3.17: Electron density profile measured by LIDAR at time t = 57.88 s with marked errorbars, the red line then indicate the absolut value of the density error

With the knowledge of the measurement density error it is possible to compute the diffusion coefficient error (which is an error due to imperfection of the measurement, not due to the numerical method used for its evaluation). With the help of the equation (3.35) I have been able to evaluate the errors of each computed value of the effective diffusion coefficient:

- **σ_D = { 0.4288; 0.6730; 0.0839}**

The estimated edge plasma effective electron diffusion coefficients along with their errorbars are plotted in the Fig.3.18.

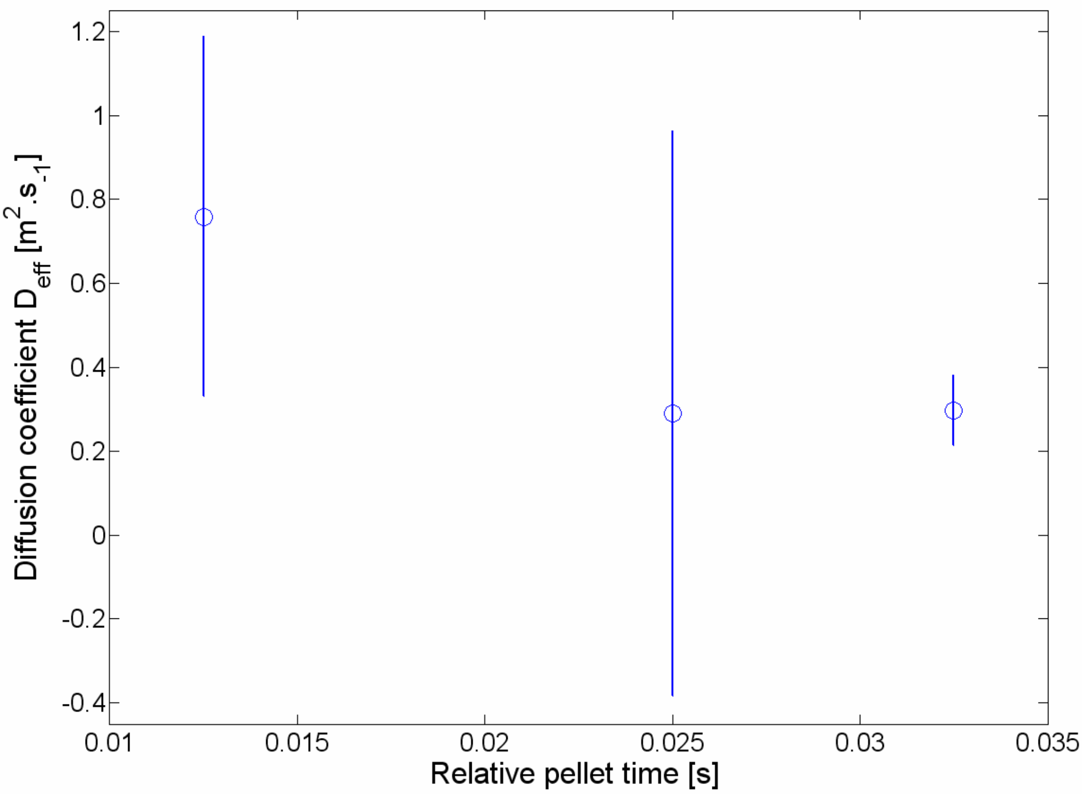

Figure 3.18: Estimated edge plasma effective electron diffusion coefficients with errorbars depending on the relative pellet time.

From the evolution of interferometer density it is clear that the post-pellet losses are faster immediately after the pellet then later on. It is this fast part which is most relevant. Our measurement shows that during this fast time interval the effective diffusivity accross the outer part of minor radius, $r/a > 0.6$, is $D_{eff} = 0.8 \pm 0.4\ m^2 \cdot s^{-1}$.

This value compares well with the data from MAST tokamak, where D_{eff} = (0.7-1.8) $m^2 \cdot s^{-1}$. [14]
The value of D_{eff} is very important as it determines the amount of fuelling needed to reach the required plasma density. The prediction of the amount of fuelling is very important for design of fusion reactors, in particular due to the fact that 50% of fuel is tritium, which is under strict regulatory control due to its radioactivity.

4 Summary

In this work, I investigated the plasma fuelling by pellet injection and its impact on plasma parameters. I familiarized with JET tokamak parameters and basics of plasma pellet fuelling. For present day and future devices, pellet injection has become a leading technique for plasma fuelling and also for controlling the plasma. High speed injection of solid fuel pellets provides efficient refuelling by deep particle deposition.

For experimental evaluation of plasma parameters I downloaded data from the JET pulse 53212. This pulse was a part of experiments undertaken at JET aimed to develop optimized pellet refuelling scenarios. Density and temperature profiles, D_α emission, averaged density and total plasma energy content have been downloaded.

In the experimental part of this work, the first task was to analyze the plasma response to the pellet injection. It has been observed that electron density strongly increases during the pellet evaporation, reaches its maximum and then drops down again, until the next pellet is injected. Pellet injection is followed by drop of the plasma energy content due to pellet induced ELM activity and also by the plasma temperature reduction. However, by interrupting the pellet string the plasma energy content is able to recover, while the density level remains elevated. Therefore by applying optimized pellet injection scenarios it is possible to achieve H-mode operations at high densities with good energy confinement. I also investigated the adiabaticity of pellet evaporation process. By comparing the plasma electron pressure profiles before and during the pellet evaporation I was able to conclude, that the process is approximately adiabatic. However, the adiabaticity of the process can be negated by quick edge plasma processes, especially ELMs.

Pellet size, along with its velocity and injection trajectory, is one of the pellet basic parameters, which determine its lifetime and penetration depth. I calculated the size of the injected pellet from the evolution of the plasma density profile. The estimated number of deuterium atoms contained in a single pellet was $N = 2.59 \cdot 10^{21}$, which well corresponds to the expected value of approximately $3 \cdot 10^{21}$.

The main aim of this work was to estimate the plasma diffusivity during the fast post-pellet particle losses. The value of edge plasma effective diffusion coefficient ($\mathrm{D_{eff}}$) is very important, because it determines the amount of fuelling needed to achieve the required value of plasma density. The edge plasma diffusivity can be calculated from the evolution of plasma density. Due to low measurement rate of the LIDAR diagnostics compared to quick pellet evaporation and post pellet density evolution, a boxcar method had to be used in order to gain sufficient time resolution of the data. Then the effective diffusion coefficient was computed from the plasma diffusion equation, while applying few simplifications and replacing the derivations by differences. The computed value of D_{eff} for the time about 1 *ms* after the pellet injection was: $D_{eff} = 0.8 \pm 0.4\ m^2 \cdot s^{-1}$. This value corresponds well to data from the MAST tokamak, where $D_{eff} = (0.7\text{-}1.8)\ m^2 \cdot s^{-1}$.

References

[1] G. McCracken, P. Stott. *Fúze, Energie vesmíru.* Mladá fronta, Praha, 2006

[2] Francis F. Chen. *Úvod do fyziky plazmatu*. Academia, 1984

[3] S.L. Milora et al. *Pellet fuelling – review paper*. Nucl. Fusion 35 (1995) 657

[4] P.Lang et al. *High density operation at JET by pellet refuelling*. Plasma Phys. Contr. Fusion 44 (2002) 1919

[5] J.Wesson. *Tokamaks*. Oxford University Press, Clarendon Press, Oxford, 2004

[6] H. W. Barthels, H.S. Bosch, R. Brakel, H.J. Hartfuss, D. Hartmann, R. Hippler, D.H.H. Hoffmann, R. Kleiber, A. Könies, K. Krieger, A. Melzer, A.G.Peeters, R. Schneider, B.D. Scott, W. Suttrop, H. Zohm. *IPP Summer University for Plasma Physics*, Greifswald, 2005

[7] T.J. Dolan. *Fusion research: Principles, experiments and technology.* Pergamon Press, 2000

[8] B. Pégourié. *Pellet injection experiments and modelling*. to be published

[9] F. Köchl. *Pellet drift effect studies at JET*. EPS Conference, Warsaw, 2007, Paper O1.143

[10] I. Senichenkov. *The pellet rocket acceleration caused by* ∇B*-induced drift*. EPS Conference, Warsaw, 2007, Poster O4.094

[11] L.R. Baylor et al. *Pellet fuelling and control of burning plasmas in ITER*. Nucl. Fusion 47 (2007) 443

[12] K. Gal. *Pellet induced perturbations in the plasma edge*. EPS Conference, Warsaw, 2007, Paper O4.080

[13] J.Limpouch. *Základy fyziky plazmatu – lecture*. KFE FJFI ČVUT v Praze

[14] M. Valovic. *Confinement characteristics of pellet-fuelled plasmas in MAST*. EPS Conference, Warsaw, 2007, Paper O4.026

[15] M. Valovic at al. *Density peaking in low collisionality ELM-y H-mode in*

JET. Plasma Phys. Contr. Fusion, 46 (2004) 1877

[16] *ITER* [online]. [cit. 2007-07-27] <http://www.iter.org>

[17] *EFDA-JET, the world's largest nuclear fusion research experiment* [online]. [cit. 2007-07-27] <http://www.jet.efda.org>

[18] J. Mlynář. *Úvod do termojaderné fúze – lecture.* KF FJFI ČVUT v Praze

[19] *Glossary of Fusion Terms* [online] [cit. 2007-07-27] <http://www.fusion.org.uk/info/glossary.htm>

Acknowledgements

At the first place I would like to thank to my supervisor Ing. Martin Valovič, Ph.D. for his support and help with my work and also for his great patience. I would also like to express my gratitude to Ing. Ivan Ďuran, Ph.D from the CASTOR tokamak for his willingness to help me with my work, whenever I was in need.